Physics – Uspekhi **58** (9) 850 – 871 (2015)

REVIEWS OF TOPICAL PROBLEMS PACS numbers: 03.50.De, 07.85.Qe, **41.60. – m**

Undulators and wigglers for the production of radiation and other applications

N A Vinokurov, E B Levichev

DOI: 10.3367/UFNe.0185.201509b.0917

Contents

Abstract. We describe periodic magnetic systems known as undulators and wigglers that are used in circular accelerators and free-electron lasers both to generate radiation and to control the beam parameters. The design details and radiation characteristics of such systems are discussed together with their influence on electron motion.

Keywords: undulators, synchrotron radiation, electron circular accelerators

N A Vinokurov Budker Institute of Nuclear Physics,
Siberian Branch of the Russian Academy of Sciences,
prosp. Akademika Lavrent'eva 11, 630090 Novosibirsk,
Russian Federation
E-mail: nikolay.vinokurov@gmail.com
Korea Atomic Energy Research Institute, 305-353 Daejeon,
Republic of Korea;
Novosibirsk State University,
ul. Pirogova 2, 630090 Novosibirsk, Russian Federation
E B Levichev Budker Institute of Nuclear Physics,
Siberian Branch of the Russian Academy of Sciences,
prosp. Akademika Lavrent'eva 11, 630090 Novosibirsk,
Russian Federation;
Novosibirsk State Technical University,
prosp. K. Marksa 20, 630073 Novosibirsk, Russian Federation

Received 20 May 2015, revised 29 June 2015
Uspekhi Fizicheskikh Nauk **185** (9) 917 – 939 (2015)
DOI: 10.3367/UFNr.0185.201509b.0917
Translated by A L Chekhov; edited by A M Semikhatov

1. Introduction

Magnets with a spatially periodic transverse field are widely used in charged-particle storage rings, colliders, synchrotron radiation (SR) sources, and free-electron lasers (FELs). The idea to use the periodic transverse motion of relativistic electrons to generate short-wave radiation was originally suggested by Ginzburg [1] in 1947. In 1951, Hans Motz from Stanford University considered the radiation from relativistic electrons moving in a periodic transverse alternating magnetic field [2]. The magnetic system that formed such a field was named the undulator by Motz (from the French *onduler*, to oscillate). In 1952, he installed the undulator in a linear accelerator and observed the undulator radiation in the millimeter and visible spectral regions [3]. The term 'wiggler' is almost a synonym for 'undulator'. In his original setup, Motz used permanent magnets, which formed a field with an amplitude of 5 kG and period of 40 mm in a 4 mm gap.

A periodic sequence of magnets (with a 'gradient') was first suggested for accelerators by Robinson [4] in 1958 and realized in 1966 at the Cambridge Electron Accelerator (CEA). It was used not for the extraction of radiation but for the redistribution of damping rates of betatron and synchrotron oscillations. Nowadays, such devices are known as Robinson wigglers.

Since that time, wigglers and undulators have mainly been used for: 1) generation of SR for experiments, electron beam diagnostics, and other applications; 2) control of the parameters of circulating beams such as the damping rate of oscillations, emittance, and the time of radiative polarization of electrons. Starting with SR sources of the third generation,

storage rings were designed in such a way that the radiation source would be predominantly undulators and wigglers. Changing the parameters of these devices allows obtaining radiation with the desired properties: spectrum, flux, brightness, divergence etc. Periodic magnetic systems can also control the beam parameters and find applications such as in damping rings, colliders, and SR sources. For example, in the third-generation SR source PETRA III (Positron–Electron Tandem Ring Accelerator III), an 80-meter-long set of wigglers with permanent magnets allowed decreasing the horizontal emittance by a factor of four, reaching the record value of 1 nm rad for the energy of 6 GeV [5]. Such a small phase space of the beam allows efficient use of the radiation from undulators installed in the straight sections of PETRA III.

2. Radiation from relativistic charged particles in the vacuum

We recall some details regarding the radiation from charged particles. We define the radius vector $\mathbf{R}_{12} = \mathbf{n}R_{12} = \mathbf{R} - \boldsymbol{\rho}$ directed from the point $\boldsymbol{\rho}$ where a point-like charge e is located, moving at the speed $\dot{\boldsymbol{\rho}} = \mathbf{v} = \boldsymbol{\beta}c$ (c is the speed of light), to the point $\mathbf{R}$ where the radiation field is measured. At large distances from the charge, $R \gg \rho$, we can assume that $\mathbf{n} \approx \mathbf{R}/R$ and $R_{12} \approx R - \mathbf{n}\boldsymbol{\rho}$. The radiation electric field then has the form [6]

$$\mathbf{E} = \frac{e}{cR}\frac{\mathbf{n}\times\left[(\mathbf{n}-\boldsymbol{\beta})\times\dot{\boldsymbol{\beta}}\right]}{(1-\mathbf{n}\boldsymbol{\beta})^3} = \frac{e}{cR}\frac{\mathrm{d}}{\mathrm{d}t}\frac{\mathbf{n}(\mathbf{n}\boldsymbol{\beta})-\boldsymbol{\beta}}{1-\mathbf{n}\boldsymbol{\beta}} = -\frac{e}{c^2}\frac{\mathrm{d}^2}{\mathrm{d}t^2}\frac{\boldsymbol{\rho}-\mathbf{n}(\mathbf{n}\boldsymbol{\rho})}{R}\,, \tag{1}$$

where the quantities in the right-hand side are evaluated at the retarded time $t' = t - R_{12}/c$. In deriving the second and the third equality in (1), we used the relation

$$\frac{\mathrm{d}t'}{\mathrm{d}t} = \frac{1}{1-\mathbf{n}\boldsymbol{\beta}}\,. \tag{2}$$

The last part of Eqn (1) shows that the radiation field is proportional to the angular acceleration of the charge position observed from the point where the field is measured [7].

2.1 Synchrotron radiation

The simplest example of synchrotron radiation[1] is the radiation emitted by a charge that rotates clockwise with a constant angular frequency Ω along a circle with radius r. We find the radiation field in the rotation plane at a point located on the x axis for simplicity (Fig. 1). In this case, the charge coordinates can be written as

$$x(t') = r\sin(\Omega t')\,,\quad y(t') = r\left[\cos(\Omega t') - 1\right],$$
$$c(t-t') = \sqrt{y^2(t') + (R - x(t'))^2} \approx R - x(t')\,,$$

and from Eqn (1) we obtain the only nonzero component of the field:

$$E_y(R,0,0,t) = \frac{e\beta^2}{Rr}\frac{\cos(\Omega t') - \beta}{\left[1-\beta\cos(\Omega t')\right]^3}\,. \tag{3}$$

[1] The term 'synchrotron radiation' (also known as magnetic bremsstrahlung radiation) is related to the fact that such radiation is observed during electron motion in synchrotrons — cyclic accelerators of charged particles.

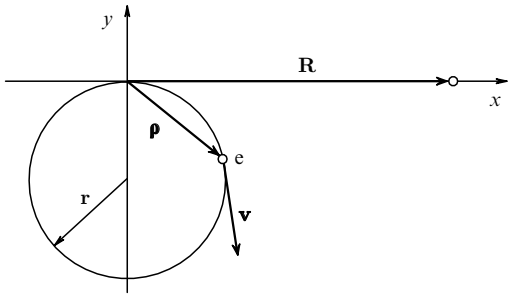

Figure 1. Charge that rotates clockwise along a circle with radius r with a constant speed v. The observer is located on the x axis.

If the rotation is slow ($v \ll c$), we can neglect the retardation during the emission time and assume that $t \approx t' + R/c$. In this case, Eqn (3) becomes the formula for ordinary dipole radiation

$$E_y(R,0,0,t) = \frac{e\Omega^2 r\cos\left[\Omega(t - R/c)\right]}{c^2 R}\,, \tag{4}$$

where the numerator contains the second derivative of the y-projection of the dipole moment.

The derivative in (2), which can be expressed as

$$\frac{\mathrm{d}t'}{\mathrm{d}t} = \frac{1}{1-\mathbf{n}\boldsymbol{\beta}} = \frac{1}{1-\mathrm{d}x(t')/\mathrm{d}t'} = \frac{1}{1-\beta\cos(\Omega t')}\,, \tag{5}$$

describes the visible irregularity of the rotation. This visible acceleration can easily be explained. Let the charge travel along a small section of the upper part of the circle (Fig. 2). The charge emits short signals at points A and B; the distance between these points is $\mathrm{d}s$. The signal is emitted from point B after the time interval $\mathrm{d}t' = \mathrm{d}s/v$. Because point A is located farther from the observer by the distance $\mathrm{d}s$, the delay for detecting the second signal equals $\mathrm{d}t = \mathrm{d}t' - \mathrm{d}s/c = \mathrm{d}t'(1-\beta)$. Such a change in the delay between two signals, caused by the finiteness of the signal (wave) propagation speed, is known as the Doppler effect. If the speeds are close to the speed of light, field (3) is significant only at phases around $\Omega t' = 2\pi n$, when the denominator in the right-hand side becomes close to zero. This means that the field is a sequence of short pulses,

$$E_y(R,0,0,t) \approx \frac{e}{rR(1-\beta)^2}\frac{1-(1-\beta)^{-1}(\Omega t')^2/2}{\left[1+(1-\beta)^{-1}(\Omega t')^2/2\right]^3}\,, \tag{6}$$

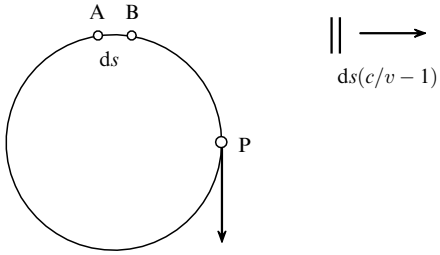

Figure 2. 'Snapshot' of the signals emitted by a charge from points A and B, shown as two vertical segments in the upper-right part of the figure. The registration delay between the signals is less than the emission delay due to different distances from the observer to points A and B.

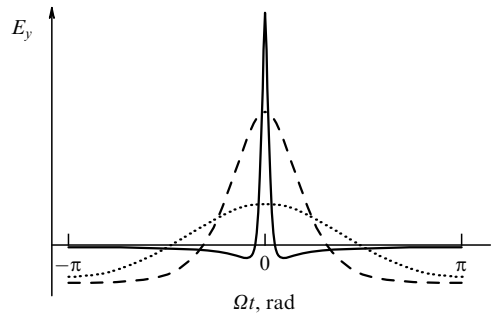

Figure 3. Radiation field versus the phase Ωt that ranges from $-\pi$ to π (that is, versus time) for $\beta = 0.05$ (dotted curve), $\beta = 0.3$ (dashed curve), and $\beta = 0.8$. For clarity, in the last two cases, the field amplitude is decreased by respective factors 20 and 1000.

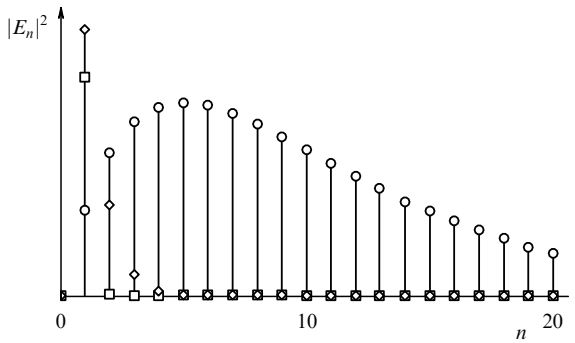

Figure 4. Radiation spectra for $\beta = 0.05$ (squares), $\beta = 0.3$ (diamonds), and $\beta = 0.8$ (circles). For clarity, the spectral intensity in the last two cases is decreased by respective factors of 1000 and 100,000.

with the repetition rate $\Omega/(2\pi)$, where

$$\frac{\Omega t'}{\sqrt{2}\sqrt{1-\beta}} \approx \sqrt[3]{(1+\tau^2)^{1/2}+\tau} - \sqrt[3]{(1+\tau^2)^{1/2}-\tau}\,, \quad (7)$$

and

$$\tau = \frac{3}{2\sqrt{2}}\,\frac{\Omega(t-R/c)}{(1-\beta)^{3/2}} \quad (8)$$

can be found from the cubic equation $r(\Omega t')^3/6 + t'(c-\Omega r) + R - ct = 0$.

Figure 3 shows the radiation electric field versus time for different speeds calculated using the exact expression (3). We can see that as the speed approaches the speed of light, the pulse duration becomes very small, according to (6), and the field amplitude $E_{\max} \approx e/[rR(1-\beta)^2]$ rapidly increases.

As follows from (6), the radiation field is relatively large only at those time instants when the charge is located near the upper point of the circle on the segment with the length (known as the radiation formation length)

$$l = r\Omega\Delta t' = r\sqrt{2}\sqrt{1-\beta} \approx \frac{r}{\gamma}\,, \quad (9)$$

where $\gamma = 1/\sqrt{1-\beta^2}$ is the relativistic factor (we assume that $\gamma \gg 1$ in what follows). With the Doppler effect taken into account, the length of these pulses can be expressed as

$$\Delta t = \frac{\mathrm{d}t}{\mathrm{d}t'}\,\Delta t' = (1-\beta)^{3/2}\,\frac{\sqrt{2}}{\Omega} \approx \frac{1}{2\gamma^3\Omega}\,, \quad (10)$$

which clearly follows from (6)–(8). By expanding field (3) in a Fourier series, we can find the radiation spectrum

$$\begin{aligned} E_n &= \frac{\Omega}{2\pi}\int_0^{2\pi/\Omega} E_y \exp(\mathrm{i}n\Omega t)\,\mathrm{d}t \\ &= \frac{\mathrm{i}n\Omega^2 e}{2\pi cR}\int_0^{2\pi/\Omega}\frac{\beta_y}{1-\beta_x}\exp(\mathrm{i}n\Omega t)\,\mathrm{d}t \\ &= -\frac{\mathrm{i}n\Omega^2\beta e}{2\pi cR}\exp\left(\frac{\mathrm{i}n\Omega R}{c}\right) \\ &\times \int_0^{2\pi/\Omega}\sin(\Omega t')\exp\left\{\mathrm{i}n\left[\Omega t' - \beta\sin(\Omega t')\right]\right\}\mathrm{d}t' \\ &= \frac{n\Omega\beta e}{cR}\exp\left(\frac{\mathrm{i}n\Omega R}{c}\right)J_n'(n\beta)\,, \end{aligned} \quad (11)$$

where J_n' is the derivative of the Bessel function. At small speeds, only the first harmonic is present in the radiation (see Eqn (3) for the dipole radiation and the dotted curve in Fig. 3). As the speed increases, higher harmonics appear. Because the radiation intensity is proportional to the square of the field, the intensity of each harmonic is proportional to the square of its amplitude.

The intensity spectra of the radiation are shown in Fig. 4 for different charge speeds. As the speed approaches the speed of light, the number of harmonics in the spectrum increases. In the ultrarelativistic case, when $n \gg 1$,

$$\begin{aligned} J_n'(n\beta) &\approx -\frac{1}{\sqrt{\pi}}\left(\frac{2}{n}\right)^{2/3}\Phi'\left[\frac{1}{\gamma^2}\left(\frac{n}{2}\right)^{2/3}\right] \\ &= \frac{1}{\sqrt{3}\pi\gamma^2}\,K_{2/3}\left(\frac{n}{3\gamma^3}\right), \end{aligned}$$

where Φ' is the derivative of the Airy function, $K_{2/3}$ is the Macdonald function of the order 2/3, and the asymptotic behavior of field harmonics (11) is expressed as

$$E_n \approx \frac{ne}{\sqrt{3}\pi\gamma^2 Rr}\,K_{2/3}\left(\frac{n}{3\gamma^3}\right)\exp\left(\frac{\mathrm{i}n\Omega R}{c}\right). \quad (12)$$

The amplitude of the harmonic is maximal for $n = 0.834n_c$, where $n_c = (3/2)\,\gamma^3 = 3/(4\Omega\Delta t)$ is the so-called critical harmonic number. The high-frequency ($n \gg n_c$) part of the spectrum has the form $|E_n|^2 \approx e^2 n\exp(-n/n_c)/(2\pi\gamma r^2 R^2)$.

In a large number of modern accelerators, the electrons can be accelerated up to relative energies of the order of $\gamma = 10^4$. In this case, according to (10), if the turning radius is $r = 10$ m, the electron emits pulses with a length of the order of $r/\gamma^3 = 10^{-11}$ m. The radiation spectrum is maximal for harmonic numbers around $n_c \sim 10^{12}$. This means that the spectrum contains all wavelengths from 20π m (the first harmonic wavelength is approximately the length of the electron trajectory) to 10^{-12} m, the length of the radiation pulse. The wavelength $\lambda_c = 2\pi r/n_c = (4\pi/3)\,r/\gamma^3$ is known as the critical wavelength of synchrotron radiation.

For ultrarelativistic ($\gamma \gg 1$) electrons, the short pulse is formed only in the vicinity of the highest point of the trajectory ($y = r$, $x = 0$). According to (6), the length of this section or formation length (9) is only a small part of the electron trajectory. We can say that the radiation that propagates along the x axis is emitted from the trajectory point where the velocity vector is parallel to the x axis. On the other hand, because all points of the section with the length r/γ contribute to the radiation field, we can say that the radiation is emitted from every point of the trajectory in the tangent direction (velocity direction) with a small angular divergence $1/\gamma$. The denominator of expression (1) for the

radiation field contains the Doppler term $(1 - \mathbf{n}\boldsymbol{\beta})$; hence, the field is relatively small at those points that are farther away from the xy plane than the distance R/γ. This means that the vertical angular divergence is also of the order of $1/\gamma$. Therefore, fast particles emit radiation predominantly in the direction tangent to their trajectory.

The formation length in the numerical example discussed above is only 1 mm. If we consider a fast electron that moves along some trajectory and its curvature radius and binormal direction vary only slightly on the formation length, then we can use all the expressions for the synchrotron radiation in describing the electron radiation. A practically important example is the magnetic systems of cyclic electron accelerators, which consist of separate magnets (where the particles travel along circular arcs) that are several meters long and the formation length is usually much shorter than this distance.

In the ultrarelativistic case, the radiation that reaches the observation point is emitted from a single point of the circular trajectory. Therefore, we can imagine a simple but very useful picture: a 'snapshot' of the locus of points where the radiation field is significant (Fig. 5).

Looking at Fig. 5, we imagine that the picture is rotating clockwise around the circle center with the angular speed Ω such that the points of the circle have a speed close to the speed of light. The curve representing the radiation wave front is characterized by the following property. A tangent to any point of the circle is perpendicular to the curve at the crossing point. Such a curve is known as the circle involute. As the picture rotates, the crossing point of the curve and a fixed tangent travels with the speed of light.

The overall pattern of synchrotron radiation can thus be visualized as follows: the radiation breaks away from the charge due to the finiteness of the propagation speed and 'flies away' in the direction of the electron velocity; in other words, it is 'driven by inertia'.

We note that Eqn (1) describes the radiation field defined as a field at a distance R from the source much longer than the size of the source. Therefore, it was assumed from the very beginning that $R \gg r$. On the other hand, as was shown above, for ultrarelativistic particles (the only case that we consider in what follows), the source is not the whole trajectory but only the formation length, which is a small arc with the length $l = r/\gamma$. Therefore, the results presented above also hold for much shorter distances, when $R \gg l$. However, this is not entirely correct for the low-frequency part of radiation with $\lambda \gg \lambda_c$. From the expansion $n(1 - \beta)\,\Omega t' + n\beta(\Omega t')^3/6$ of the phase of the exponential in the expression for the Fourier harmonic amplitude (11), we can see that the first term in the expansion can be neglected for $n \ll n_c$, and only an arc $\Omega t' \sim n^{-1/3}$ contributes to the amplitude. Therefore, for harmonics with $n \ll n_c$, the formation length $l_n = rn^{-1/3}$ is larger than $l = r/\gamma$, and the condition for the observation point to be in the far field takes the form $R \gg l_n$. Correspondingly, the minimal angular divergence of the radiation is not of the order of $1/\gamma$, but instead $\sqrt{\lambda/l_n} \sim n^{-1/3}$, just as for any extended coherent source.

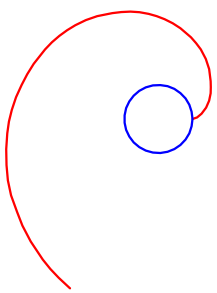

Figure 5. Radiation is located near the electron rotation plane and its wave front has the form of a spiral (circle involute).

In general, an interesting feature of the low-frequency part ($n \ll n_c$) of the synchrotron radiation spectrum is its independence from the particle energy. Indeed, if we assume that $\beta = 1$ in (11) (or $n_c \to \infty$), we obtain

$$E_n \approx \sqrt[6]{\frac{3}{4}}\,\Gamma\left(\frac{2}{3}\right)\frac{e}{\pi r R}\,\sqrt[3]{n}\,\exp\left(\frac{in\Omega R}{c}\right), \tag{13}$$

where Γ is the Euler gamma function.

The amplitude of the synchrotron radiation 'burst' can be quite large. For example, setting $R \approx r/(2\gamma)$, we obtain $E_{\max} \approx 8\gamma^5 e/r^2$. It is interesting that in the reference frame that moves along the x axis, this field is equal to the electrostatic field of a charge at the distance $r(1 - \beta)$ between the electron and the cylinder whose surface moves with the speed of light as it rotates (in the laboratory reference frame) with the frequency Ω (this surface is the event horizon in a comoving rotating reference frame). We can say that the field 'breaks away' from the charge on the surface of this cylinder.

2.2 Radiation from a charge moving along a sinusoidal trajectory

As was shown in Section 2.1, during the motion of a relativistic electron along a circle, the detected radiation is formed on the formation length r/γ, which is a small part of the whole trajectory. If we intend to use this radiation, we should increase its intensity. This can be achieved by collecting the radiation from different points of the electron trajectory. Because the high-frequency part of SR is mostly emitted in the direction of the electron motion, the optimal trajectory should deviate slightly from the direction in which we want to increase the intensity. The simplest and most common in practical applications is the sinusoidal trajectory with the period $\lambda_w = 2\pi/k_w$, described by the equations

$$x = \frac{1}{k_w^2 r}\cos(k_w z), \quad y = 0. \tag{14}$$

For such a trajectory, the radiation is emitted in the z axis direction near the points $z = n\pi/k_w$ (n is an integer), where the velocity is parallel to the z axis. The trajectory curvature at these points is $\mathrm{d}^2x/\mathrm{d}z^2 = (-1)^{n+1}/r$. Because it is quite difficult to deviate relativistic particles from a straight trajectory (besides, this is not necessary, because, according to (9), the radiation formation angle $1/\gamma$ is small), we assume in what follows that the minimal curvature radius of the trajectory r is much larger than the period: $k_w r \gg 1$. In this case, the oscillation amplitude for the angle $(\mathrm{d}x/\mathrm{d}z)_{\max} = 1/(k_w r)$ is small.

For radiation that propagates along the z axis,

$$\frac{\mathrm{d}t'}{\mathrm{d}t} = \frac{1}{1 - \beta_z} \approx \frac{2\gamma^2}{1 + K_0^2 \sin^2(k_w z)}, \tag{15}$$

where we introduce the notation

$$K_0 = \frac{1}{\sqrt{2}}\,\frac{1}{k_w r\sqrt{1 - \beta}} \approx \frac{\gamma}{k_w r}, \tag{16}$$

and the field has the only component

$$E_x(0,0,R,t) = \frac{e}{Rr(1-\beta)^2}\,\frac{1-K_0^2\sin^2(k_\mathrm{w}z)}{\left[1+K_0^2\sin^2(k_\mathrm{w}z)\right]^3}\cos(k_\mathrm{w}z)\,. \tag{17}$$

Because $c(t-t') = R - z$, the value of z is related to t as

$$k_\mathrm{w}z\left(1+\frac{K_0^2}{2}\right) - \frac{K_0^2}{4}\sin(2k_\mathrm{w}z) = 2\gamma^2 k_\mathrm{w}(ct-R)\,. \tag{18}$$

We can see from (17) that field maxima correspond to acceleration maxima that are located at the trajectory deviation maxima $z = n\lambda_\mathrm{w}/2$ and have the same value as in the case of synchrotron radiation (6) emitted by a charge that moves along the circle with radius r. The parameter K_0 introduced in (16) is the ratio of the trajectory period divided by 2π to the radiation formation length. As was mentioned above, most of the energy is emitted into a cone with the angle $1/\gamma$. Taking into account that $1/(k_\mathrm{w}r)$ is the oscillation amplitude of the angle between the velocity and the z axis, we can see that K_0 also describes the ratio of the maximal angle of the trajectory deviation to the characteristic angular divergence of the radiation (Fig. 6).

The time dependence of the radiation field is described by expression (17), with $z(t)$ found from Eqn (18). The calculation can be easily done numerically, but it is instructive to have analytic expressions. Field (17) has the period 2π with respect to the 'phase' $k_\mathrm{w}z$; therefore, the time period can be found from (18) as

$$T = \frac{\lambda_\mathrm{w}}{c}\,(1-\beta)\left(1+\frac{K_0^2}{2}\right) \approx \frac{\lambda_\mathrm{w}}{2\gamma^2 c}\left(1+\frac{K_0^2}{2}\right). \tag{19}$$

For $K_0 \gg 1$, the curvature radius varies slightly along the formation length r/γ, and the equations in Section 2.1 hold. This can be proved directly by expanding (18) in a series in $k_\mathrm{w}z$ up to the cubic term and the numerator and denominator in (17) up to the quadratic term. We then once again obtain expressions (6) and (7) for SR. This means that the radiation pulses emitted from even (sinusoid maxima) and odd (sinusoid minima) points of the sinusoid have opposite signs, as shown in Fig. 4. This time dependence of the radiation field is schematically shown in Fig. 7.

The time interval between the subsequent positive pulses is the period of our signal. It is useful to find this period in another way, similar to how we found the Doppler contraction by the factor $(1-\beta)$ for the delay between the registration of signals with respect to the delay between their emissions (see Fig. 2). However, we now have to take into account that the trajectory is not straight and the electron trajectory becomes longer than the length of the segment along which the light propagates. Indeed,

$$T = \int_0^{\lambda_\mathrm{w}} \frac{\mathrm{d}z}{v_z} - \frac{\lambda_\mathrm{w}}{c} \approx \frac{\lambda_\mathrm{w}}{c}\left(1-\beta+\frac{1}{4k_\mathrm{w}^2 r^2}\right)$$
$$\approx \frac{\lambda_\mathrm{w}}{2\gamma^2 c}\left(1+\frac{K_0^2}{2}\right). \tag{20}$$

Expression (20) shows that the time interval between the arrival of pulses from two adjacent deviation maxima of the electron sinusoidal trajectory is $1/(1-\langle\beta_z\rangle)$ times the difference between the corresponding emission times, where $\langle\beta_z\rangle = \beta - 1/(4k_\mathrm{w}^2r^2)$ is the average speed along z axis. Sometimes, the electron is considered in the reference frame where its average speed is zero and it performs periodical motion along a figure-eight trajectory. In this case, the relativistic term $\gamma_{\|} = 1/(1-\langle\beta_z\rangle^2)^{1/2} \approx \gamma/(1+K_0^2/2)^{1/2}$ is used and (19) takes the form $cT = \lambda_\mathrm{w}/(2\gamma_{\|}^2)$.

By comparing the pulse length of synchrotron radiation (10) with the delay $T/2$ between adjacent pulses, we can see that these pulses do not overlap if $K_0 \gg 1$. In this case, the spectrum of the signal, shown in Fig. 7, is similar to the synchrotron radiation spectrum, but it has no even harmonics of the fundamental frequency $2\pi/T$ and the intensity of the odd harmonics is four times higher. Moreover, the sinusoidal part of the electron trajectory in a real wiggler always has a finite length L that fits $N = L/\lambda_\mathrm{w}$ periods. The radiation pulse shown in Fig. 7 has the same number of periods. Such a signal is not periodic and its spectrum is continuous. The spectrum is similar to the discrete spectrum of a signal with an infinite number of periods, but each harmonic of the discrete spectrum corresponds to a spectral line with the width $\Delta\omega \sim 2\pi/\delta t$, where $\delta t = NT$ is the full length of the signal.

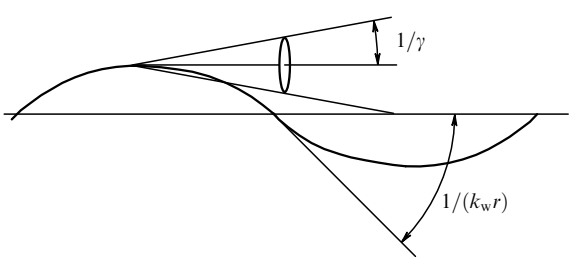

Figure 6. Two characteristic angles for the radiation of a particle that moves along a sinusoidal trajectory; the angle $1/\gamma$ of the radiation cone and the amplitude $1/(k_\mathrm{w}r)$ of angle oscillations.

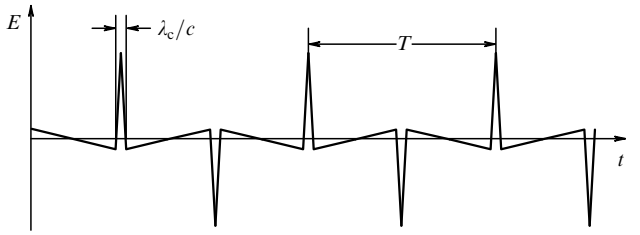

Figure 7. Time dependence of the field for the radiation emitted from the wiggler, $T/2 \gg \lambda_\mathrm{c}/c$.

2.3 Motion of a charged particle in a magnetic field

In following the laws of electrodynamics, which allowed us to find the field from a given motion of the charge, we were not interested in the forces that caused the acceleration of the charged particle. For example, uniform rotation of a charge can be achieved by fixing a charged object to a thread. For the deflection of the charged particle, an electromagnetic field can be used. The full expression for the Lorentz force

$$\mathbf{F} = e(\mathbf{E} + \boldsymbol{\beta} \times \mathbf{B}) \tag{21}$$

contains the electric $\mathbf{E}$ and magnetic $\mathbf{B}$ fields. It turns out that for static (constant in time) fields, the second term in the right-hand side of (21), proportional to the magnetic field, can be much larger than the first one. Indeed, the maximal achievable value of the electrostatic field is related to the breakdown

on the surface of the solid medium inside which the domain with the field is confined. This value is of the order of 10^7 V m$^{-1} \approx 300$ G (0.03 T). High magnetic fields are produced by permanent magnets, electromagnets with iron cores, and superconducting and pulsed electromagnets. In the first two cases, the field, which is limited by the maximal magnetization (dipole magnetic moment per unit volume) of the medium, reaches values of the order of 1 T. In the last two cases, the field is limited by the strength of the conducting coils, which are forced by the magnetic field. In this case, the maximal value of the field is of the order of 10 and 100 T.[2] Therefore, the trajectories of relativistic particles are usually controlled by a magnetostatic field. We can see from expression (21) for the Lorentz force that the magnetic part of the force is perpendicular to the velocity and therefore does not change the energy of the particle or the absolute value of the electron velocity. A particle with a mass m and momentum $p = \gamma mv$ moves in the magnetic field along the trajectory with the curvature radius $r = pc/(eB_\perp)$, where $B_\perp$ is the component of the magnetic field perpendicular to the velocity.

To realize sinusoidal trajectory (14), we should place the particle in a magnetic field that has only a vertical component in the xz plane:

$$B_y = B_0 \cos(k_w z) . \tag{22}$$

Then $r = pc/(eB_0)$ and

$$K_0 = \frac{eB_0}{k_w mc^2} \sqrt{\frac{1+\beta}{2\beta^2}} .$$

For ultrarelativistic particles, the square root in the last expression is very close to unity; therefore, in all calculations, instead of K_0, we use the parameter $K = eB_0/(k_w mc^2)$, which depends only on the amplitude and period of the magnetic field.

Because field (22) can be described by the vector potential $A_x = (B_0/k_w) \sin(k_w z)$, the parameter K is sometimes called the dimensionless vector potential.

We also note that for the generation of radiation, we use the lightest charged particles, electrons. Therefore, we assume in what follows that e and m are the charge and mass of the electron and $K \approx B_0 \lambda_w/(10.7 \text{ kG cm}) \approx 0.934\, B_0\,[\text{T}]\, \lambda_w\,[\text{cm}]$. Additionally, we note that K is the ratio of the cyclotron frequency $eB_0/(mc)$ to the frequency $2\pi c/\lambda_w$ that corresponds to the undulator period.

3. Wigglers and undulators

As was mentioned in the Introduction, a magnetic system that forms alternating periodical magnetic field (22) is called an undulator or, more specifically, a planar undulator, because the trajectory of a charged particle in it can lie in the xz plane. Often, the term 'wiggler' is used instead of 'undulator', usually for undulators with a small number of periods. Moreover, the parameter K (also known as the undulator parameter) is typically assumed to be much larger than unity for wigglers because, as discussed in Section 2, the wiggler radiation spectrum for $K \gg 1$ is similar to the synchrotron radiation spectrum. Therefore, it is sometimes assumed that the fields of radiation from different points of a wiggler do not interfere. Obviously, this is not fully correct. Interference always occurs and the spectrum of radiation from a multipole wiggler, as was mentioned above, differs from the synchrotron radiation spectrum (in the wiggler spectrum, there are lines with the $2\pi/T$ spacing and even harmonics disappear for the radiation emitted along the z axis). On the other hand, if $K \gg 1$, this frequency period is rather small and the spectral lines are broadened due to the velocity spread in the electron beam and because the radiation is usually collected from the solid angle (which is not small compared with λ/L) around the z axis direction, where the radiation field period is larger (see Section 3.2). In this case, the radiation spectrum coincides with the spectrum of SR from a single field maximum and the spectral intensity of the radiation is proportional to the number of wiggler periods N. This gives reason to speak about the absence of interference for the total radiation summed over all electrons in a beam and collected from a finite aperture.

3.1 Spectrum of the forward radiation

As we can see from Fig. 6, only a small part of the trajectory contributes to the field of wiggler radiation. To obtain the maximal number of radiation sources at a given length of a wiggler, we can keep the curvature radius r constant (keep the maximal magnetic field B_0 constant) and decrease the wiggler period λ_w to the point where the peaks of the synchrotron radiation, shown in Fig. 7, start to overlap, and the field amplitude starts decreasing. As follows from (10) and (19), this happens when $r/\gamma \approx \lambda_w/(2\pi)$ or when $K \approx 1$. In most cases, the undulator period cannot be reduced to the optimal value $2\pi r/\gamma$, because this also decreases the amplitude of the magnetic field, which, in turn, causes the SR burst length to increase together with the radiation critical wavelength $\lambda_c = (4\pi/3)\, r/\gamma^3 = 4\pi mc^2/(3eB_0\gamma^2)$.

This means that for practical applications, the most interesting case is where $K \sim 1$ and the 'bursts' of radiation from different maxima of the magnetic field start to overlap. In this case, the number of harmonics of the fundamental frequency $2\pi/T$ in the radiation spectrum decreases. If radiation field period (19) is known, then, using expression (17), it is easy to find the (odd) field harmonics:

$$\begin{aligned}
E_n &= -\frac{2\pi i n e}{cT^2 k_w r R} \int_0^T \frac{\beta_z \sin(k_w z)}{1-\beta_z} \exp\left(\frac{i2\pi n t}{T}\right) dt \\
&= -\frac{2\pi i n e}{c^2 T^2 k_w r R} \int_0^{\lambda_w} \sin(k_w z) \exp\left(\frac{i2\pi n t}{T}\right) dz \\
&= -\frac{2\pi i n e}{c^2 T^2 k_w^2 r R} \exp\left(\frac{i2\pi n R}{cT}\right) \int_0^{2\pi} \sin\varphi \\
&\times \exp\left\{ in\left[\varphi - \frac{K^2}{4+2K^2} \sin(2\varphi)\right]\right\} d\varphi \\
&= \frac{2\gamma^4 n e}{(1+K^2/2)^2 r R} \left[J_{(n-1)/2}\left(\frac{nK^2}{4+2K^2}\right) \right. \\
&\left. - J_{(n+1)/2}\left(\frac{nK^2}{4+2K^2}\right)\right] \exp\left(\frac{i2\pi n R}{cT}\right) .
\end{aligned} \tag{23}$$

It follows from (23) that if $K \ll 1$, the harmonics rapidly decrease as the number n increases, leaving practically only the first harmonic. Moreover, Eqns (18) and (23) show that the emergence of higher harmonics in the radiation spectrum

[2] Because the magnetic field pressure in the vacuum is simply its energy density $\mathbf{B}^2/(8\pi)$, we can easily calculate that a field of 100 T (10^6 G) produces a pressure of 4 kN mm^{-2}. This value should be compared with the yield strength of the magnetic coil material, copper: 0.4 kN mm^{-2}.

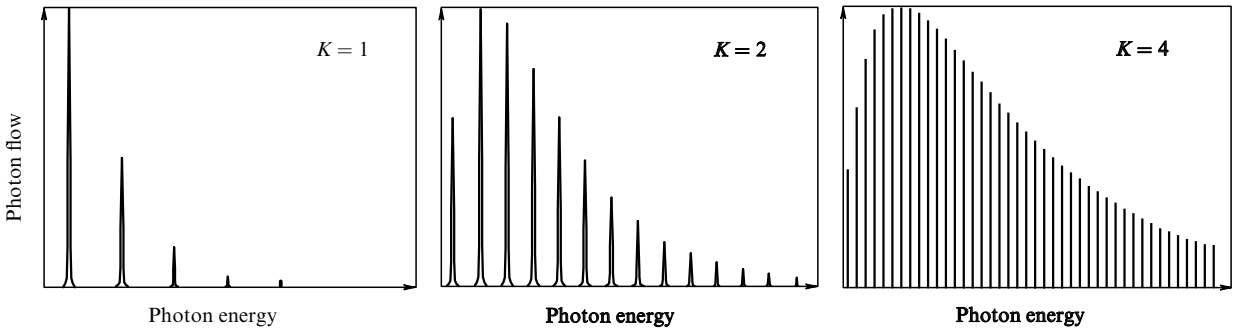

Figure 8. Characteristic form of the spectra for radiation from a long wiggler with different values of the undulator parameter K.

as K increases is connected with the modulation of the longitudinal velocity, proportional to K^2. When $K > 1$, the wavelength of the first harmonic increases together with the number of harmonics in the spectrum, and when $K \gg 1$, the radiation harmonics have such a small spacing that their envelope approaches the continuous spectrum of the SR generated by a bending magnet (Fig. 8). Precisely in this case is a periodic magnet called a wiggler.

The above analysis of the radiation spectrum from a wiggler leads to a simple way of approximately optimizing the wiggler. We assume that we need to obtain radiation with the maximal spectral intensity per unit length of the wiggler at a wavelength λ. We first consider a wiggler with a period that is much larger than $2\gamma_{||}^2\lambda$. Then, according to (19) and (23), the number cT/λ of the harmonic that we are interested in is large and, in order to obtain a significant intensity, we need $K > 1$. In this case, we can apply equations for SR. Because the short-wave part (12) of the SR spectrum decreases exponentially, by equating the specified wavelength λ to the critical one $\lambda_c = (4\pi/3)\, r/\gamma^3 \approx 4\pi mc^2/(3eB_0\gamma^2)$, we can obtain the minimum required magnetic field:

$$B_0 = \frac{4\pi mc^2}{3e\lambda\gamma^2} \approx \frac{7\ \text{kG cm}}{\lambda\gamma^2}\,. \tag{24}$$

Relation (24) can also be used to find the minimum electron energy

$$\gamma_{\min} = \sqrt{\frac{4\pi mc^2}{3eB_0\lambda}} \approx \sqrt{\frac{7\ \text{kG cm}}{B_0\lambda}} \tag{25}$$

that is needed for generating radiation in the specified magnetic field. It only remains to design a wiggler with the field and the minimum period such that the number of SR sources per unit length be maximal.

3.2 Spatial distribution of undulator radiation

Undulator radiation away from the z axis is also easy to find. Instead of (18), we have

$$c(t - t') \approx R - \frac{n_x}{k_w^2 r}\cos(k_w z) - z n_z\,. \tag{26}$$

Then

$$\frac{\mathrm{d}t}{\mathrm{d}t'} = 1 - \beta_z n_z + \frac{\beta_z n_x}{k_w r}\sin(k_w z)\,, \tag{27}$$

and the spatial period (first harmonic wavelength) of the radiation field can be obtain by integrating (27) over the undulator period:

$$\lambda_1 = cT = \int_0^{\lambda_w} \frac{\mathrm{d}t}{\mathrm{d}t'}\frac{\mathrm{d}z}{\beta_z} = \int_0^{\lambda_w}\frac{\mathrm{d}z}{\beta_z} - \lambda_w n_z$$
$$\approx \lambda_w\left(1 - \cos\theta + \frac{1}{2\gamma_{||}^2}\right), \tag{28}$$

where the unit vector projection $n_z = \cos\theta$ is expressed in terms of the angle θ between the radiation direction and the z axis. This expression generalizes expression (19) for the wavelength of the first harmonic of undulator radiation.

The angular dependence of the undulator radiation wavelength has a simple geometric explanation. We consider two wave fronts (surfaces of constant phase) that correspond, for example, to acceleration maxima (undulator field maxima). Subsequently passing through different field maxima, the particle emits spherical waves.[3] The center of each sphere is located at its source, as shown in Fig. 9. In this case, the wavelength of the first harmonic, that is, the distance between two adjacent wave fronts, is expressed as

$$\lambda_1 = cT = \lambda_w\left(\frac{1}{\langle\beta_z\rangle} - \cos\theta\right) \approx \lambda_w\left(1 - \cos\theta + \frac{1}{2\gamma_{||}^2}\right). \tag{29}$$

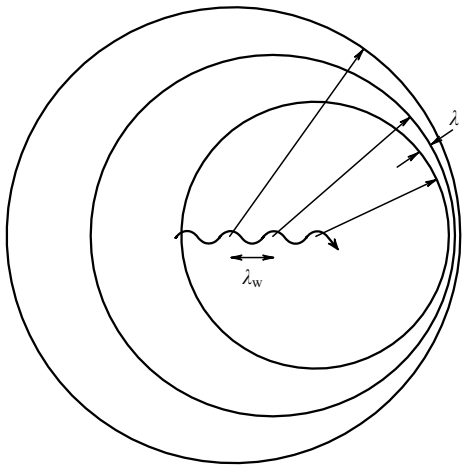

Figure 9. Wave fronts emitted from different field maxima. The wavelength of forward radiation is minimal.

[3] This reasoning is reminiscent of the Huygens principle, but in this case the source of the spherical wave is every point of the electron trajectory, instead of every point of the wave front.

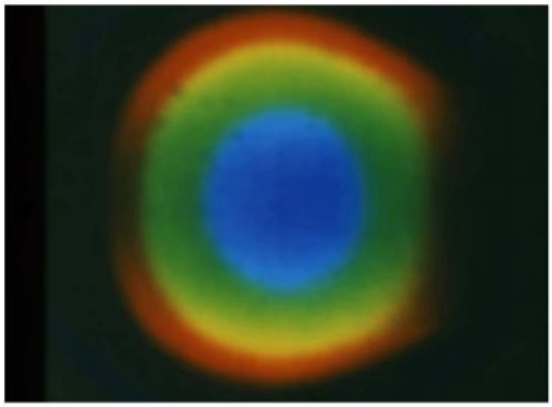

Figure 10. (Color online.) Spontaneous undulator radiation. The size of the spot in the photograph is limited by the fact that the film used (as well as the eye) is sensitive only to visible light (0.4–0.8 μm). Invisible infrared radiation is incident outside the red fringe. The first harmonic wavelength of the forward radiation is $\lambda_1(\theta = 0) \approx 0.4$ μm.

If we substitute $1/\langle\beta_z\rangle \to \cos\theta_i$, expression (29) transforms into the condition for wave reflection, when the wave is incident at the angle θ_i on a diffraction grating with the period λ_w. This is not surprising because (29) is also a condition for the spatial synchronism,

$$k_z = \frac{2\pi}{T\langle v_z\rangle} - k_w\,, \tag{30}$$

of three waves: 1) the wave emitted with a longitudinal component of the wave vector $k_z = (2\pi/\lambda_1)\cos\theta$; 2) the Fourier harmonic of the space charge with the wave vector $2\pi/(\langle v_z\rangle T)$ (the first term in the right-hand side of (30)); 3) a static periodical structure — the undulator with the wave vector k_w (the second term in the right-hand side of (30)).

It follows from (28) that the radiation wavelength increases together with the distance from the z axis along which the electron moves. By placing a photographic plate on the z axis far from the source, we can obtain the picture shown in Fig. 10.

3.3 Undulator radiation in the comoving reference frame

It is useful to consider undulator radiation from the standpoint of the observer moving along the z axis with the same average speed $\langle v_z\rangle$ as the electron does (Fig. 11).

The swing of electron transverse oscillations $x_{max} = 1/(k_w^2 r)$ is the same as in the laboratory frame and the period $2\pi/\omega_c = \lambda_w/(\gamma_{||}\langle v_z\rangle)$, as well as the wiggler field period, contract by the factor $\gamma_{||}$. We note that the electron oscillation frequency ω_c is $\gamma_{||}$ times higher than in the laboratory frame. The wiggler field increases by a factor of $\gamma_{||}$ and the horizontal transverse electric field $E_x = \gamma_{||}B_0\cos\left[\gamma_{||}k_w(z + \langle v_z\rangle t)\right]$ appears, causing transverse oscillations of the electron. Because $\langle v_z\rangle \approx c$, the wiggler field becomes similar to a monochromatic plane wave with linear polarization. The horizontal component v_x of the electron velocity oscillates with the amplitude $cK/(1 + K^2)^{1/2}$. For small K, this amplitude is much smaller than the speed of light. This means that in this case, the radiation is that of a dipole and the radiation distribution in the comoving reference frame is very simple. The electric field is

$$E(R, \varphi, t) = \frac{e\omega_c^2 x_{max}}{c^2 R}\sin\varphi\cos\left[\omega_c\left(t - \frac{R}{c}\right)\right], \tag{31}$$

where φ is the angle between the x axis, along which the charge oscillates, and the direction from the origin, near which the charge is located, to the observation point. The radiation has the same frequency for all directions, equal to the charge oscillation frequency ω_c. The amplitude of the field and hence the radiation intensity is zero on the x axis. After the transformation from the comoving reference frame to the laboratory one, the radiation in the x axis direction transforms into radiation that propagates at the angle $1/\gamma_{||}$ to the z axis. Therefore, the intensity in Fig. 10 is attenuated on the left-hand and right-hand sides from the center (but does not vanish because K was not small and higher harmonics were present in this experiment). Lorentz transformations applied to this transition result in a frequency that corresponds to wavelength (29).

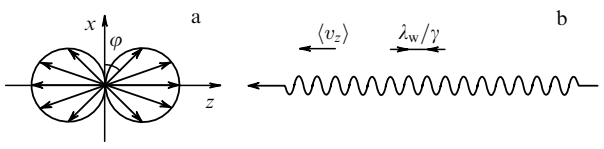

Figure 11. Undulator radiation in the comoving reference frame. (a) Directivity pattern of dipole radiation (more precisely, its cross section by the xz plane). The length of the arrows whose ends are located at the circles are proportional to the amplitude of the radiation field in the corresponding direction. (b) Undulator field approaching an electron with the speed $\langle v_z\rangle$.

3.4 Compton scattering

As was already mentioned, the radiation field depends only on the charge motion, not on the forces that caused this motion. The above-discussed charge oscillations along the x axis can be caused by the field of a plane monochromatic electromagnetic wave that propagates, for example, along the z axis in the negative direction, $E_x = E_0\cos(k_c z + \omega_c t)$. In the comoving frame, the situation is very similar to the one shown in Fig. 11, but the speed of the wave is c instead of $\langle v_z\rangle$ and the wavelength is $2\pi c/\omega_c$. In this case, the wave is said to scatter on the charge. The energy of the wave that approaches the charge along the z axis is then assumed to diverge in all directions from the charge, according to (31). The scattering of the wave on the charge is called Thomson or Compton scattering.[4] The quantitative measure for the scattering is the ratio of the scattered power to the intensity of the plane wave incident on the electron, that is, the Thomson scattering cross section. In the laboratory reference frame, the frequency of the incident plane wave is $2\gamma_{||}$ times less than that of the comoving one; therefore, the frequency of the backscattered radiation is $4\gamma_{||}^2$ times the frequency of the scattered wave.

For example, if a laser with a wavelength of 1 μm radiates towards an electron beam with an energy of 1 GeV ($\gamma \approx 2000$), then the energy of the backscattered photons is around 20 MeV. Such photons are used in nuclear physics

[4] Arthur Compton showed theoretically and experimentally that at high frequencies, the frequency of light initially scattered by an electron at rest is smaller than the frequency of the incident wave. This frequency shift, called the Compton effect, was one of the first experimental confirmations of quantum theory.

experiments [8, 9]. We can say that in the method described above for producing gamma rays, we replaced the undulator with a magnetostatic field by the traveling wave of laser radiation. The dimensionless vector potential of the electromagnetic wave with the amplitude E is

$$K = \frac{eE}{k_0 mc^2} \approx \sqrt{\frac{I\lambda_0^2}{(14\ \text{GW})}},$$

where I is the intensity and λ_0 is the wavelength (instead of λ_w for the undulator). Usually, this potential is small. We note that due to the diffraction limitations of the light beam size, the quantity $I\lambda_0^2$ is of the order of the minimum power that can provide the intensity I for optimal focusing. Therefore, generating a light beam with $K > 1$ at a length of at least several wavelengths requires power higher than 100 GW. The invention of lasers with high peak power allowed obtaining waves with $K > 1$, which opened new laser application fields, in particular, laser acceleration (see, e.g., [10, 11]).

It may seem that we can now replace undulators with lasers and use accelerators (including laser ones) that are several orders of magnitude cheaper with a lower energy $\gamma = \sqrt{\lambda_0/\lambda_1}/2$ of electrons. This is still not possible due to the small length of the laser pulse. Indeed, according to (17) and (23), the radiation field for a given wavelength λ_1 and $K \sim 1$ is proportional to the electron energy or $\sqrt{\lambda_0}$, and because the angular divergence is $1/\gamma$, the full power of the radiation does not depend on the 'undulator' wavelength. The pulse length of high-power lasers does not usually exceed 0.1 ns, and the typical undulator transit time L/c is 10 ns; therefore, a laser source with the same peak power (for the same electron currents) emits two orders of magnitude less energy. The loss in the average power is even higher. Modern electron storage rings provide electron beams with an average current up to several amperes, consisting of bunches with the repetition rate of the order of 100 MHz. Magnetostatic undulators installed in storage rings allow obtaining radiation with an average power up to 100 kW for the hard X-ray range and 1 kW for the vacuum-ultraviolet range.

Despite the progress in laser technology, 'laser undulators' would hardly be able to compete in the coming years with magnetostatic ones in the field of radiation generation with high average power.

3.5 Helical undulators

We consider the superposition of two planar undulator fields,

$$B_x = B_0 \sin(k_w z), \quad B_y = B_0 \cos(k_w z), \tag{32}$$

which is the transverse field whose vector rotates as the z coordinate changes. With suitable initial conditions, the electron moves in such a field along a spiral trajectory

$$x = \frac{1}{k_w^2 r}\cos(k_w z), \quad y = -\frac{1}{k_w^2 r}\sin(k_w z). \tag{33}$$

Because the longitudinal speed $\beta_z = 1 - (1+K^2)/(2\gamma^2)$ is constant, the radiation directed along the z axis consists of only the first harmonic with the wavelength

$$\lambda_1 = cT = \frac{\lambda_w}{2\gamma^2}(1+K^2) \tag{34}$$

and the amplitude components

$$\begin{aligned} E_{x1} &= -\frac{2\pi i e}{cT^2 k_w r R}\int_0^T \frac{\beta_z \sin(k_w z)}{1-\beta_z}\exp\left(\frac{i2\pi t}{T}\right)\mathrm{d}t \\ &= \frac{2\gamma^4 e}{(1+K^2)^2 rR}\exp\left(\frac{i2\pi R}{cT}\right), \\ E_{y1} &= -\frac{2\pi i e}{cT^2 k_w r R}\int_0^T \frac{\beta_z \cos(k_w z)}{1-\beta_z}\exp\left(\frac{i2\pi t}{T}\right)\mathrm{d}t \\ &= \frac{2i\gamma^4 e}{(1+K^2)^2 rR}\exp\left(\frac{i2\pi R}{cT}\right). \end{aligned} \tag{35}$$

This means that the radiation is circularly polarized, which is obvious because the radiation field, according to (1), is proportional to the transversal acceleration.

A charged particle can move along spiral trajectory (33) not only in transverse magnetic field (32). This trajectory can be achieved in a uniform longitudinal magnetic field $B_z \approx \gamma k_w mc^2/e$ if the initial conditions are $x(0) = 1/(k_w^2 r)$, $x'(0) = y(0) = 0$, $y'(0) = -1/(k_w r)$. In this sense, the solenoid that creates such a longitudinal field can be treated as an undulator. However, some distinctions between such an 'undulator' and an undulator with a transverse field must be noted.

First, for high electron energies, the trajectory period for realistically attainable fields increases greatly, which does not allow using solenoids for the generation of radiation with wavelengths shorter than 0.1 mm. In this case, the power of spontaneous radiation is low. A corresponding electronic device that uses stimulated radiation is called a relativistic cyclotron resonance maser. Second, the parameters of the spiral trajectory in the longitudinal field significantly depend on the initial conditions. In particular, the angular dispersion of an electron beam leads to a significant dispersion of the longitudinal speed and the corresponding broadening of the radiation spectrum. A combination of a solenoid and a transverse field undulator is sometimes used in long-wave free-electron lasers or ubitrons.

Useful and interesting properties of synchrotron and undulator radiation can be found in [12–18]. A description of the application of undulators for obtaining stimulated undulator radiation (that is, free-electron lasers) is beyond the scope of this review. A relatively simple introduction to the physics of free-electron lasers can be found in [19].

4. Magnetic field of an undulator

Both electromagnets and permanent magnets are used to create the magnetic field in wigglers and undulators. A comparison of different technologies can be found in [18, 20]. Permanent magnets are mainly used in the construction of short-period undulators for cyclic SR sources as well as for FELs. Because the field of a permanent magnet is proportional to the magnetic moment per unit volume of the material, the scaling of the device dimensions does not influence the magnitude of the field. This allows creating smaller (inexpensive and easy to fabricate) models of undulators with permanent magnets in order to study their characteristics. In the case of electromagnets, according to the equation $\mathrm{rot}\,\mathbf{H} = 4\pi\mathbf{j}/c$, the reduction in size (with a constant current density $\mathbf{j}$) leads to the same reduction in the field strength. Therefore, electromagnetic undulators with a reasonable field amplitude have quite a large period, and the

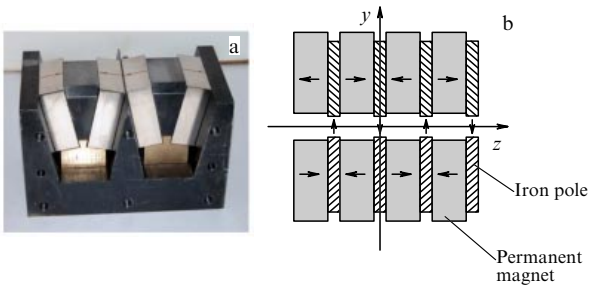

Figure 12. (a) Model of an undulator with permanent magnets (lower part of an undulator) without sidewalls. Wedge-shaped iron poles allow concentrating the magnetic flux and increasing the amplitude of the field in the gap. (b) Scheme of a hybrid undulator.

reduction of the period leads to the reduction of the field strength in the gap. Field amplitude values higher than 1 T for periods of 3–10 cm can be reliably obtained only when permanent magnets are used. The situation for superconducting magnets is the same as for electromagnets, but because the achievable current densities are 100 times higher, the amplitude of the field can be substantially larger.

Figure 12 shows a model of the lower half (one period) of a planar undulator with permanent magnets. Here, so-called hybrid technology is used [21, 22], according to which magnetic blocks alternate with poles made from a soft magnetic material, which closes the magnetic flux.

Figure 13 shows an electromagnetic undulator and its cross section in the yz plane. The undulator consists of a magnetic conductor with poles (made of soft magnetic materials — low-carbon electrotechnical steel or Co-Fe-alloys with high saturation flux density), between which the coils are located. Because there are no currents in the working gap of an undulator, the field in this region can be obtained using the periodic scalar magnetic potential $\psi(x, y, z) = \psi(x, y, z + \lambda_w)$,

$$\mathbf{B} = \operatorname{grad}\psi\,, \quad \Delta\psi = 0\,. \tag{36}$$

For the devices shown in Fig. 12 and 13, the potential satisfies the symmetry conditions

$$\begin{aligned}\psi(x, y, z) &= -\psi\left(x, y, z + \frac{\lambda_w}{2}\right) = \psi(x, y, -z)\\ &= -\psi(x, -y, z) = \psi(-x, y, z)\,.\end{aligned} \tag{37}$$

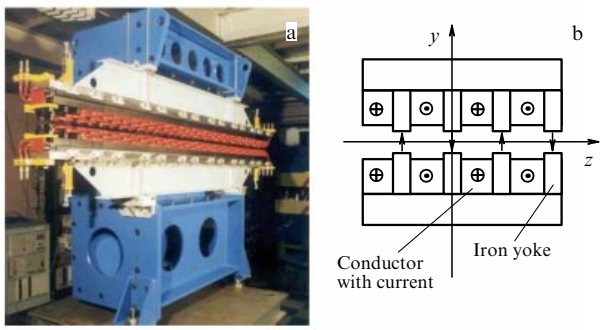

Figure 13. (Color online.) (a) Electromagnetic undulator (coils are in red). (b) Diagram of the electromagnetic undulator cross-section.

The poles of undulators and wigglers are usually made wide enough in the horizontal direction, such that the potential in the working region does not depend on x. In this case, the periodic solution of Laplace equation (36) with symmetry conditions (37) has the simple form

$$\psi = \sum_{n=0}^{\infty} \frac{B_n}{(2n+1)\,k_w} \cos\left[(2n+1)\,k_w z\right] \sinh\left[(2n+1)\,k_w y\right]. \tag{38}$$

We note that due to symmetry conditions (37), the magnetic field in the undulator gap contains only odd harmonics. To calculate the amplitude of a harmonic B_n, we need to know the potential on the boundary of the vertical aperture of the undulator for $y = \pm g/2$. The characteristic form of the potential $\psi(g/2, z)$ is shown in Fig. 14.

The undulator poles correspond to flat regions in Fig. 14, because the unsaturated iron details are equipotential with good accuracy (the strength of the magnetic field inside them is small in comparison with that outside). For a hybrid undulator, the pole potential is $\psi_0 = Ht/2$, where H is the strength of the magnetic field in the permanent magnet and t the thickness of the magnet in the direction of magnetization, that is, along the z axis. For an electromagnet, the pole potential is $\psi_0 = 2\pi I/c$, where I is the total current in the gap between two adjacent poles.

The scalar potential at the boundary can be expressed as a Fourier series:

$$\psi\left(\frac{g}{2}\,, z\right) = \sum_{n=0}^{\infty} a_n \cos\left[(2n+1)\,k_w z\right]. \tag{39}$$

With (38), this allows finding the field harmonic amplitudes on the axis:

$$B_n = \frac{(2n+1)\,k_w a_n}{\sinh\left[(2n+1)\,k_w g/2\right]}\,. \tag{40}$$

It follows from expression (40) that in an undulator with a short period ($k_w g > 1$), the amplitudes of the harmonics decrease rapidly as the number n increases. By approximating the dependence (see Fig. 14) of the potential at the boundary between adjacent poles with a straight line, we can estimate the amplitude of the first harmonic,

$$B_0 \approx \frac{H}{\sinh\left(\pi g/\lambda_w\right)} \frac{4}{\pi} \sin\frac{\pi t}{\lambda_w}\,. \tag{41}$$

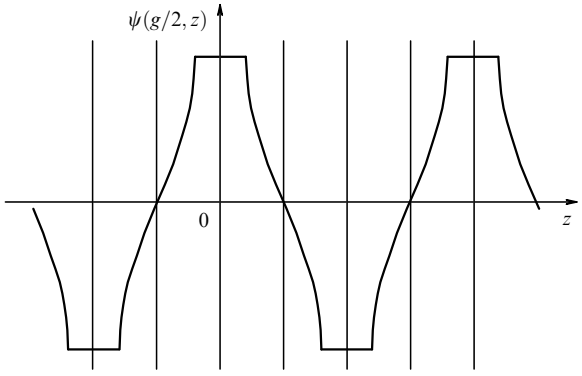

Figure 14. Scalar potential $\psi(g/2, z)$ at the boundary.

The field strength H in a permanent magnet is slightly less than the coercive force H_c, even for large heights of the magnet. The magnetization M of modern hard magnetic materials (for example, Nd-Fe-B) is almost independent of the field and $H_c \approx B_r \approx 14$ kG, where $B_r = 4\pi M$ is the residual induction.[5] The maximum thickness of a permanent magnet equals half the undulator period, but the soft magnetic poles cannot be too thin, due to the saturation. Therefore, a good estimate for the permanent magnets of an undulator is $t/\lambda_w \approx 0.3$ and $H/B_r \approx 0.8$. Then Eqn (41) yields

$$B_0 \approx 0.8\,\frac{B_r}{\sinh\left(k_w g/2\right)}\,. \tag{42}$$

Expression (42), despite its simplicity, gives a good estimate of the field of hybrid undulators with a short period.

Using wedge-shaped poles [23] (Fig. 12a), the thickness of the poles can be reduced far from the working gap, where the field inside them is smaller. This decreases the undesired fluxes from the sidewalls of the pole, which allows concentrating the magnetic flux in the working gap and increasing the undulator field by 10% – 20%.

An inherent limit for both hybrid and electromagnetic undulators is the saturation of the soft magnetic pole. Therefore, the field on the axis of an electromagnetic device is usually bounded by the 2 T (besides, the period should be long enough, and it is therefore more correct to speak about a wiggler, but not an undulator). An attempt to increase the field always encounters the problem of cooling the coil with a large current density. In permanent magnet wigglers or superconducting devices, the field amplitudes can be much higher. For example, in the asymmetric wiggler ESRF (European Synchrotron Radiation Facility) [24], a field of 3.57 T was obtained for an aperture of 6 mm. At the Budker Institute of Nuclear Physics, SB RAS, several wigglers with fields up to 10 T were designed and fabricated [25].

The design of permanent magnet undulators without soft magnetic materials is even simpler. An example of such a design for a planar undulator is shown in Fig. 15.

The field on the axis of this undulator can be calculated by summing the fields of all hard magnetic material blocks under the assumption that the magnetization $B_r/(4\pi)$ does not depend on the field [26]:

$$B_0 = \frac{4\sqrt{2}}{\pi}\,B_r \exp\left(-k_w\,\frac{g}{2}\right)\left[1 - \exp\left(-k_w h\right)\right], \tag{43}$$

where h is the height of the magnetic block. Comparing (43) with (41) and (42) shows that for relatively small periods ($\pi g/\lambda_w > 1$), the fields are approximately the same, but for higher periods the hybrid constructions produce a higher field. This is because the saturating magnetic field B_s of the pole material (iron or permendur) is approximately 2 T and this value is slightly higher than B_r of modern hard magnetic materials. The relation between the corresponding magnetizations $B_s/(4\pi)$ and $B_r/(4\pi)$ is the same.

Under the condition $\pi g/\lambda_w > 1$, scalar potential (38) can be approximately expressed as

$$\psi \approx \frac{B_0}{k_w}\cos\left(k_w z\right)\sinh\left(k_w y\right). \tag{44}$$

If the approximation of an infinitely broad pole turns out to be insufficient for a planar undulator, the dependence on the horizontal coordinate x is introduced in (44):

$$\psi \approx \frac{B_0}{k_y}\cos\left(k_w z\right)\sinh\left(k_y y\right)\cosh\left(k_x x\right), \tag{45}$$

where $k_x^2 + k_y^2 = k_w^2$. The parameter k_x characterizes the transverse dependence of the magnetic field (for example, $k_x = 0$ for an infinitely broad pole or k_x is imaginary for a narrow pole and is real for a 'concave' pole, when the interpolar gap is maximal in the transversal direction for $x = 0$).

We note that analytic expressions for the magnetic field of a wiggler or undulator can be reasonably used only for estimations. For real engineering, software for three-dimensional modeling of the magnetic field should be used.

As follows from (41)–(43), the field in the gap exponentially decreases if the undulator period is small. Therefore, it is almost meaningless to design an undulator with the period smaller than the gap. The minimum width of the gap is usually limited by the effects that occur when the electron beam passes through it: loss of peripheral particles, currents induced in the walls of the vacuum chamber, heating of the vacuum chamber by undulator radiation, and other effects. Usually, the minimum width of the gap is of the order of 1 cm. Permanent magnet undulators are relatively simple and inexpensive. In comparison with nonsuperconducting electromagnetic undulators, they provide a shorter period with a higher field amplitude. Larger fields can be obtained by using superconducting technologies [27–31]. However, superconducting magnets are quite complicated and expensive, both in realization and service, which prevents their wide use.

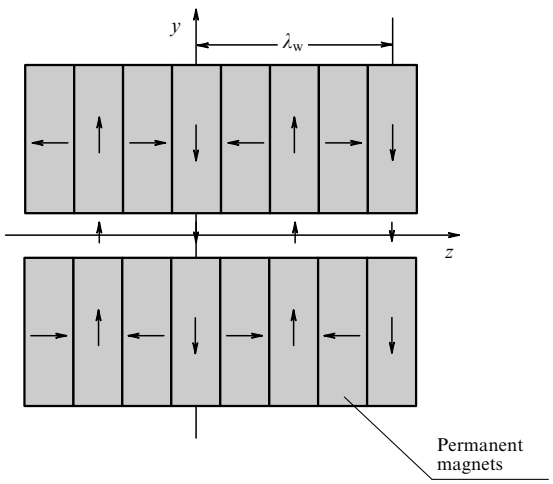

Figure 15. Plane undulator with permanent magnets.

5. Experiments with the undulator radiation of a single electron

The high brightness of the radiation provided by a long undulator in the VEPP-3[6] electron circular accelerator allowed performing a set of unique experiments on the study

[5] We recall that the vectors of magnetic induction **B** and magnetic field **H** in hard magnetic materials are directed oppositely in the operating range.

[6] VEPP, the Russian abbreviation for counter-propagating electron–positron beams.

of the influence of synchrotron-radiation quantum fluctuations on the motion of a single electron circulating in the circular accelerator. We recall (see books [32–34]) that electrons in a circular accelerator move along a closed equilibrium orbit. The energy losses due to radiation are compensated when the electrons pass through the gap with a longitudinal electric field. This field is alternating in time harmonically. In this case, we can imagine a particle that always passes the accelerating gap at the instant when the energy increment at the gap matches the energy losses per cycle. The energy of this particle, called the reference particle, can be defined using the condition that its period of revolution be a multiple of the voltage period in the gap, because the period of particle revolution in the circular accelerator depends on the particle energy. If the initial energy or arrival time of an electron slightly differs from corresponding values for the reference particle, then the deviation of these values from the reference ones oscillate (this effect is known as autophasing). The time delay is associated with the coordinate, and the energy deviation is associated with the momentum. These oscillations are damped by the radiation reaction force. On the other hand, the oscillations are excited by instantaneous radiative energy losses via the emission of single photons with the energy $\hbar\omega$ [35, 36]. These two processes of excitation (called quantum fluctuations of radiation) and damping result in a Gaussian distribution of the electron delay and energy deviation. The length of the electron bunch and the energy spread have been measured repeatedly in many electron circular accelerators and have shown good agreement with the calculated values.

We note that the calculations were performed using the semiclassical picture of radiation discussed above. The radiation is represented as a sequence of instantaneous photon emissions with a specific energy at specific time moments. This does not agree with the uncertainty relation. As is known, the interaction of an electron with the electromagnetic field is continuous in quantum (as well as in classical) electrodynamics and is described by continuous equations with no 'jumps'. The reasoning about the wave packet reduction during measurement, which is often used in quantum theory, is not applicable to this problem. Of course, the considered system (an electron in a circular accelerator) is open, and the emitted radiation carries some information on the electron state. Therefore, this situation is similar to the case of continuous fuzzy measurement. On the other hand, there is no macroscopic measuring device. Moreover, the wave packets that describe electrons have to spread during the long particle lifetime in the circular accelerator. If the interaction with the field prevents spreading, a question of the size of the density matrix localization length arises.

These questions motivated researchers to perform single-electron experiments in the VEPP-3 circular accelerator at the INP, SB RAS [37–40]. The experimental setup is shown in Fig. 16a. An electron moved in the circular accelerator with a 7-m-long undulator installed in one of the straight segments. Undulator radiation was incident on the photomultiplier tube with a pulse length of several nanoseconds. The driving generator of a high-frequency accelerating system generated reference pulses with the frequency of revolution (4 MHz). Every photocount pulse (triggering of the photomultiplier tube) launched a device that measured time intervals and the first subsequent reference pulse stopped it.

The time dependence of the measured photocount delays is shown in Fig. 16b. We can clearly see that most of the

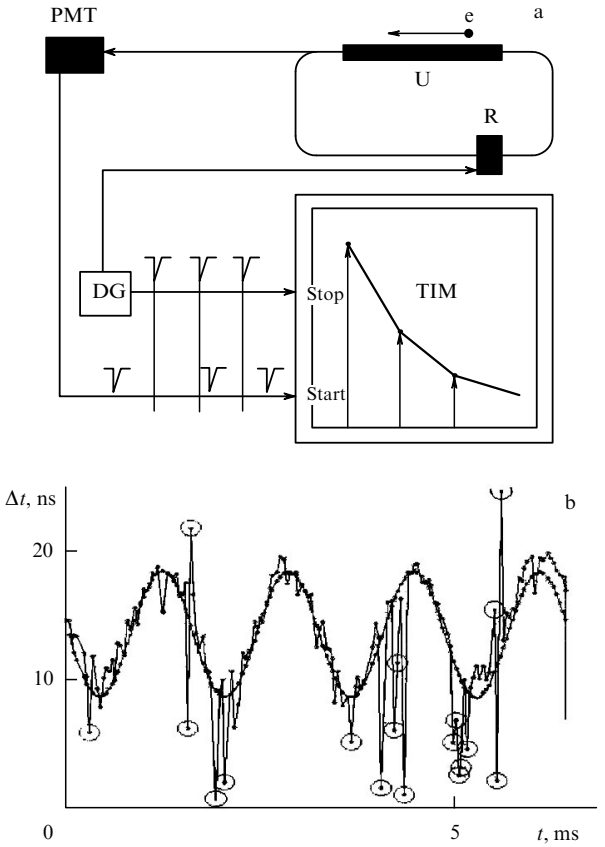

Figure 16. (a) Experimental setup for the time measurement of photocounts for single-electron undulator radiation in a circular accelerator. U — undulator, R — accelerating high-frequency resonator, DG — driving generator of the accelerating system, PMT — photomultiplier tube, operating in the counting regime, TIM — time interval meter, launched by the PMT pulse and stopped by the DG pulse. (b) Time dependence of the delay Δt (points connected with line segments) between the photocount and the nearest subsequent reference pulse. The sinusoidal fit was found using the least square method; excluded points are indicated by circles.

photocounts (points) lie on the sinusoid. In order to use the least square method for fitting, points with an offset greater than three standard deviations were excluded (nonlinear filtering). These points corresponded to total noise of the photomultiplier tube (that is, the signal without an electron in the circular accelerator). The frequency of the sinusoid coincided with the calculated value (around 1 kHz) of synchrotron oscillation frequency.

Usually, every set of measurements, which took several seconds, contained several tens of thousands of photocounts. The decay time of synchrotron oscillations was around 0.1 s. The obtained long sequence of photocount delays was divided into segments with a length of several synchrotron oscillation periods. The amplitude and phase of the sinusoid (that is, the amplitude and phase of the electron synchrotron oscillations) was obtained for every segment using the least square method. The average synchrotron oscillation frequency $\langle\Omega\rangle$ was then calculated and the regular part of the phase $\langle\Omega\rangle t$ was subtracted from the measured phase. The resulting sequence of amplitudes and slow phases is plotted in polar coordinates in Fig. 17. These points form trajectories in the phase plane of electron longitudinal motion.

These results prove that electron motion is chaotic. This fact can be explained by the influence of energy loss

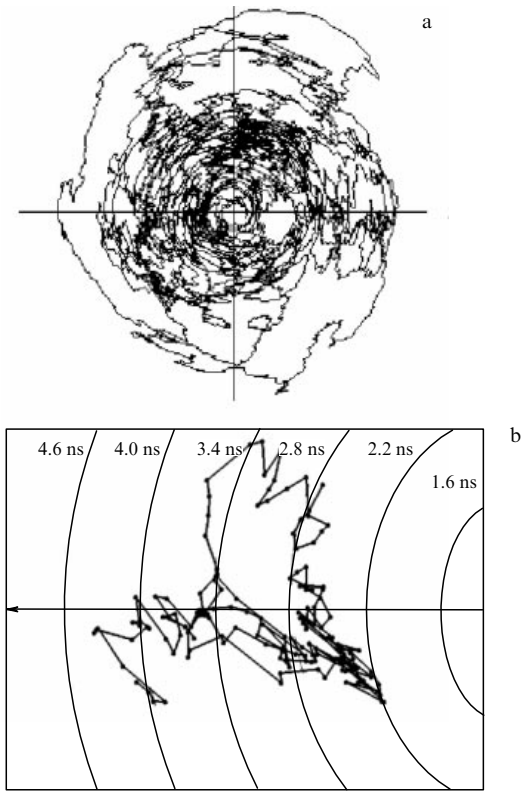

Figure 17. (a) Electron trajectory on the phase plane of longitudinal motion. (b) Close-up of the phase trajectory part from Fig. a.

fluctuations, which are a 'random' component of the radiation reaction force. Similar measurements were performed for two electrons in a circular accelerator. It was shown that the forces that act on different electrons are practically noncorrelated. This means that the small contribution to the observed random forces from 'technical' noises (in the high-frequency and magnetic systems of the circular accelerator) is negligible.

Points close in time that form phase trajectories in Fig. 17 are located not far from each other. This demonstrates both the high resolution of the measurement and the high degree of electron localization (with respect to the average amplitude of oscillations). As was mentioned above, this is not obvious. Synchrotron oscillations in a circular accelerator are nonlinear, and their frequency depends on the amplitude. Therefore, at small and large amplitudes, we can see the rotation in Fig. 17a (directed oppositely, because the rotation with the time-averaged frequency is subtracted). In the case of a quantum nonlinear pendulum, according to the uncertainty relation, there is always some amplitude spread. Therefore, if the initial phase spread is small, it increases linearly in time. This increase is similar to the spreading of a wave packet in free space. The electron can stay in the circular accelerator for several hours, and without interaction with the radiation field its wave function (or density matrix) would be quite uniformly distributed over the synchrotron oscillation phases.

The experiment described shows that the electron is well localized with respect to the phase, which slowly varies due to the interaction with the radiation field. Localization was also proved in the intensity autocorrelation measurements, performed using a modified Brown–Twiss interferometer. In this experiment, the undulator radiation of a single electron was distributed between two photomultiplier tubes by a semitransparent mirror and the delay between two photocounts was measured. A nonzero delay is possible only for a nonlocalized electron. However, such events were observed only below the noise level, and the main peak of the photocount delay distribution was at the zero value, having a width equal to the time resolution of the photomultiplier tube (around 1 ns). Most likely, localization is caused by the radiation process. Unfortunately, there are no quantum electrodynamic calculations for the density matrix (including nondiagonal elements) of the electron in a circular accelerator (an estimate for the localization length can be found in [41, 42]). This is not surprising because we consider the stationary state (radiative energy losses are constantly compensated by the electric field in the accelerating gap) and, apparently, the problem cannot be solved in the framework of the perturbation theory.

Another interesting feature of electron motion in a circular accelerator is its 'true randomness'. The electron motion (Fig. 17b) is such as if it were influenced by a random force described by the semiclassical theory for quantum fluctuations of synchrotron radiation. The trajectory shown in Fig. 17b is similar to that of a small particle in a liquid (Brownian motion). However, these random motions have a different nature. The Brownian motion trajectory is not 'truly random', because, in principle, knowing the initial velocities of molecules of the liquid, it would be possible to calculate both the motions of these molecules and the motion of the particle during the collisions. The 'randomness' of Brownian motion is related to the absence of information on microscopic initial conditions (microscopic parameters of the system). However, in electron motion, all initial conditions (microscopic parameters) are known (all electromagnetic field oscillators are in the ground state), but the electron motion is fundamentally unpredictable.

To summarize the experiments conducted give one of a few examples of a truly random process. These experimental results, in particular, prove the fundamental unpredictability of the future (failure of Laplacian determinism), demonstrating that 'God does play dice'.

6. Wigglers and some of their applications in accelerator technology

For a large undulator parameter $K \gg 1$, the wiggler spectrum almost coincides with the spectrum of a bending magnet with the critical energy

$$\varepsilon_c\,[\mathrm{keV}] = 0.665 B\,[\mathrm{T}]\, E^2\,[\mathrm{GeV}^2]\,. \tag{46}$$

The absence of strong constructive interference between radiation emitted from different points of the trajectory leads to the fact that the intensity of SR generated in an N-period wiggler is just increased by a factor of $2N$ with respect to the radiation produced by a magnet with the field B. The large horizontal angle of the beam orbit deviation in a wiggler, $\pm\theta_m = \pm K/\gamma$, allows separating the radiation into a set of output channels that can be used in a number of different experimental stations. The critical energy of SR emitted at the angle θ to the wiggler axis is described by the expression

$$\varepsilon_c(\theta) = \varepsilon_c(0)\sqrt{1 - \left(\frac{\theta\gamma}{K}\right)^2}\,. \tag{47}$$

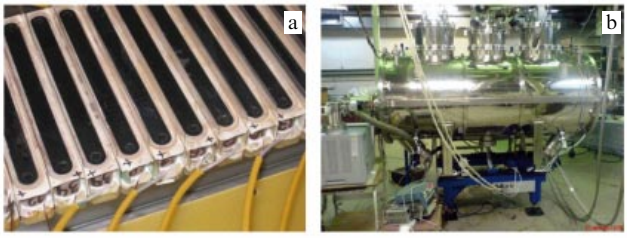

Figure 18. Superconducting wigglers fabricated at the INP SB RAS. (a) part of a yoke from a multipole wiggler with a small period used at Canadian Light Source (CLS). (b) Wiggler with a large field amplitude in a cryostat for SR source Sibir 2 (NRC "Kurchatov Institute").

Every year, wigglers with a large number of poles (small field period) are becoming more popular because they produce a higher flux and brightness of radiation. Because experiments require quanta with relatively high energy (50–100 keV), superconducting magnets are used more often. However, just as in undulators, both permanent and electric magnets are used.

Figure 18a shows a piece of a yoke from a multipole superconducting wiggler used at Canadian Light Source (CLS), with the small period $\lambda_w = 34$ mm and the field amplitude $B_0 = 2$ T [43]. Figure 18b illustrates the wiggler in a cryostat used at the SR source Sibir 2 of the National Research Center "Kurchatov Institute" ($\lambda_w = 200$ mm, $B_0 = 7.5$ T).

Reducing the wiggler field period leads to interference effects in the radiation, especially at large wavelengths. The calculated radiation spectrum (Fig. 19) for the CLS SR source shows that at photon energies higher than $\approx 3-4$ keV, SR characteristics are close to those in an ordinary magnet. At the same time, the long-wave radiation demonstrates discrete harmonics typical of an undulator.

Based on the experience of INP SB RAS in fabricating superconducting multipole wigglers [44], the amplitude of the magnetic field can be expressed as a function of the pole gap g and the wiggler period λ_w [45]:

$$B_0 \approx 12 \exp\left[-\pi\frac{g}{\lambda_w} - 2.2\left(\frac{g}{\lambda_w}\right)^2\right] [\mathrm{T}]. \qquad (48)$$

This empiric expression holds for $g \approx 8-40$ mm and $\lambda_w \approx 10-100$ mm.

Wigglers, unlike undulators, are used not only as experimental sources of SR but also to control electron beam properties. A strong spatially inhomogeneous field can strongly influence the beam dynamics (for example, shift the betatron oscillation frequency) or its radiative parameters.

One of the most popular areas of this research field is the reduction of the beam damping time (which is important for damping storage rings) or emittance (which is important for SR sources). As an example, we consider a system of damping permanent-magnet wigglers with a total length of 80 m, which was designed and fabricated by the INP SB RAS for the PETRA III SR source (German Electron Synchrotron, DESY) with the beam energy 6 GeV [5]. Twenty wigglers with the parameters $\lambda_w = 0.2$ m, $B_0 = 1.5$ T, and radiation power 400 kW (at 100 mA current) allowed decreasing the horizontal emittance by four times, i.e., to $\varepsilon_x = 1$ nm, which is a record value for such electron energies. A sequence of damping wigglers in the straight segment of PETRA III is shown in Fig. 20.

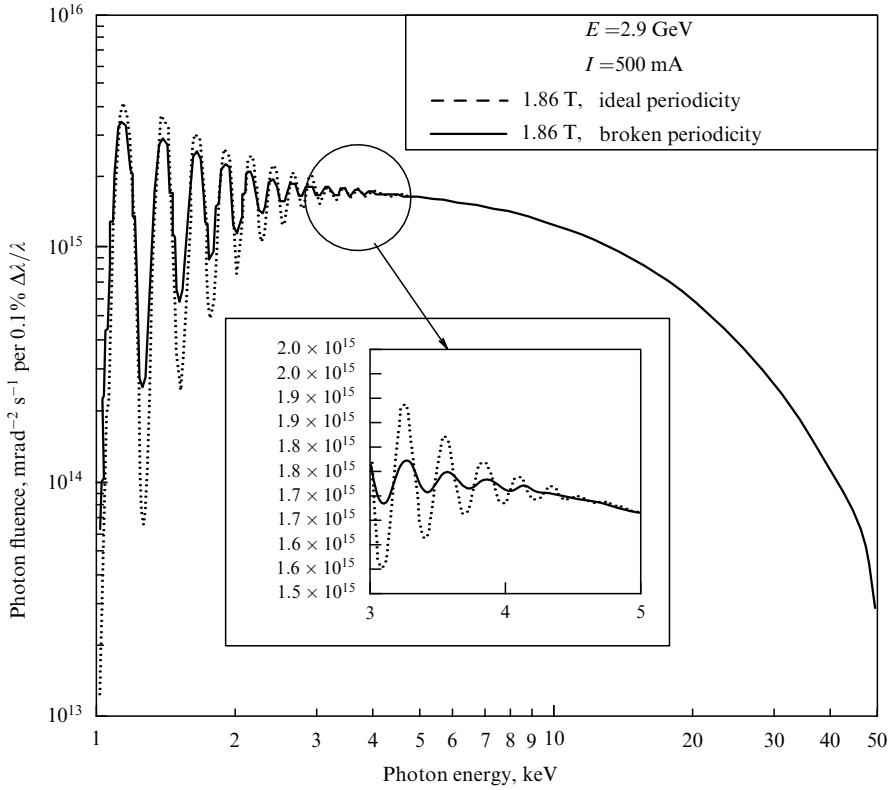

Figure 19. Spectrum of radiation from a multipole wiggler with a small field period.

Figure 20. Damping wigglers installed at the PETRA III SR source.

6.1 Wiggler influence on optics and beam dynamics

In the simple case of a planar wiggler with a sinusoidal field (see Section 2.3), the initial velocities and coordinates of the electron can be chosen such that it would move along sinusoidal trajectory (14). The trajectory is more complicated for other initial conditions. To find this trajectory, we write the longitudinal momentum in the paraxial approximation:

$$p_z = \sqrt{p^2 - \left(P_x - \frac{e}{c}\,A_x\right)^2 - \left(P_y - \frac{e}{c}\,A_y\right)^2}$$

$$\approx p - \frac{(P_x - eA_x/c)^2 + (P_y - eA_y/c)^2}{2p}\,, \qquad (49)$$

where $A_x = \int B_y\,\mathrm{d}z$, $A_y = -\int B_x\,\mathrm{d}z$ are the nonzero components of the vector potential, and P_x and P_y are the generalized momenta. Assuming the longitudinal component z to be an independent variable, we use $-p_z$ from (49) as a Hamiltonian. Under the assumption of a rapidly oscillating wiggler field, after averaging over rapid oscillations, we obtain the effective Hamiltonian

$$H = p - p_z = \frac{P_x^2 + P_y^2}{2p} + \frac{\left\langle (eA_x/c)^2 + (eA_y/c)^2 \right\rangle}{2p}\,, \qquad (50)$$

where angular brackets denote averaging over the wiggler period. The meaning of Hamiltonian (50) is simple. Electron motion consists of a slow motion, described by averaged transverse momenta P_x and P_y, and a rapidly oscillating motion, related to terms proportional to the vector potential. Then the average kinetic energy of rapid oscillations is the potential energy for the averaged motion. The last statement is a multidimensional generalization of the Kapitza method for describing motion in a rapidly oscillating field [46].[7] In our case, this statement is quite demonstrative, because the sum of kinetic energies for slow and rapid motions is on average equal to the total energy, which is constant.

After passing to average angles $p_x = P_x/p$ and $p_y = P_y/p$, substituting the explicit expressions for the vector potential found from scalar potential (45), and expanding in a series in the deviation from the z axis through the fourth term, we obtain the Hamiltonian [47]

$$H_\mathrm{w} = \frac{1}{2}\,(p_x^2 + p_y^2) + \frac{1}{4}\,\theta_\mathrm{m}^2 (k_x^2 x^2 + k_y^2 y^2)$$

$$+ \frac{1}{12}\,\theta_\mathrm{m}^2 (k_x^4 x^4 + 3k_x^2 k_\mathrm{w}^2 x^2 y^2 + k_y^4 y^4)\,. \qquad (51)$$

We recall that k_x determines the form and size of the field dependence on the horizontal transverse coordinate x (if such dependence is absent, then $k_x = 0$) and $k_\mathrm{w}^2 = k_x^2 + k_y^2$. The trajectory equations follow from (51):

$$\frac{\mathrm{d}^2 x}{\mathrm{d}z^2} + \frac{\theta_\mathrm{m}^2 k_x^2}{2}\,x + \frac{\theta_\mathrm{m}^2}{6}\,(2k_x^4 x^3 + 3k_x^2 k_\mathrm{w}^2 x y^2) = 0\,,$$

$$\frac{\mathrm{d}^2 y}{\mathrm{d}z^2} + \frac{\theta_\mathrm{m}^2 k_y^2}{2}\,y + \frac{\theta_\mathrm{m}^2}{6}\,(2k_y^4 y^3 + 3k_x^2 k_\mathrm{w}^2 x^2 y) = 0\,. \qquad (52)$$

As follows from (52), terms quadratic in coordinates in the second brackets in the right-hand side of (51) describe the focusing properties of the wiggler field, while the fourth-order terms [in the third brackets in (51)] describe the nonlinearity of this focusing. The presence of the small coefficient $\theta_\mathrm{m}^2 \ll 1$ shows that in most cases the wiggler or undulator influence on the beam dynamics is relatively small and can be treated as a small correction to unperturbed betatron oscillations in the electron circular accelerator. Using the restoring force weakness in (52), integrating (52), and neglecting the coordinate variation during the electron transit through the wiggler, we can estimate the optical powers (inverse focal distances) of the wiggler:

$$\frac{1}{F_x} \equiv -\frac{\Delta(\mathrm{d}x/\mathrm{d}z)}{x} = \frac{\theta_\mathrm{m}^2 k_x^2}{2}\,L\,,$$

$$\frac{1}{F_y} \equiv -\frac{\Delta(\mathrm{d}y/\mathrm{d}z)}{y} = \frac{\theta_\mathrm{m}^2 k_y^2}{2}\,L\,. \qquad (53)$$

Nonlinear terms in (52) describe aberrations of this astigmatic lens.

Small additional focusing in the electron circular accelerator shifts betatron frequencies by $\Delta\nu_{x,y} = \bar{\beta}_{x,y}/(4\pi F_{x,y})$, where $\beta_{x,y}$ are functions of the longitudinal coordinate along the closed electron circular accelerator orbit that characterize the transverse focusing of electrons by the main magnetic system of the circular accelerator (so-called betatron functions or beta-functions), and the overbar denotes averaging over the longitudinal coordinate along the wiggler length. In the case of an infinitely wide pole, $k_x = 0$ and the shift of the horizontal frequency disappears, just as for a bending magnet with parallel edges: focusing by the homogeneous field and defocusing by the magnet edge fully compensate each other. The vertical frequency shift does not depend on the wiggler period in this case and is expressed as

$$\Delta\nu_y \approx \frac{L\bar{\beta}_y}{8\pi r^2}\,. \qquad (54)$$

If the field and/or the wiggler length are large enough and the beam energy is small, the betatron oscillation frequency can change significantly ($\Delta\nu_y \sim 0.1-0.5$) and distort the behavior of betatron functions. This effect can be compensated by reducing $\bar{\beta}_y$ and adjusting the frequency shift together with optical function distortion, using quadrupole lenses.

[7] The corresponding multidimensional generalization presented in textbook [46] is incorrect.

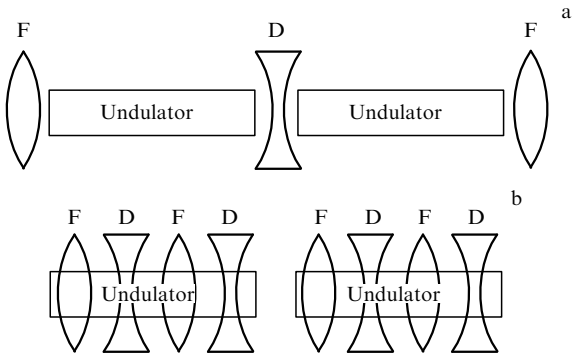

Figure 21. FODO-cell for placing wigglers and undulators with separated (a) and combined (b) functions.

The simplest focusing system for a long wiggler consists of quadrupole lenses placed between wiggler sections. A sequence of lenses with the alternating sign of $\partial B_y/\partial x$ (so-called FODO structure [8]) is the simplest cell for placing wigglers and undulators (Fig. 21a) and was used, for example, in the one-hundred-meter undulator of the X-ray free electron laser LCLS (Linac Coherent Light Source) [48]. If the undulator is long enough, an additional focusing is sometimes introduced inside it (Fig. 21b). Such structures were also successfully used earlier [49, 50]. The disadvantage of built-in quadrupoles is, obviously, the complicated design.

Other, more complicated, cells with two or three lenses placed between wigglers [51] can be used instead of FODO, and they allow obtaining a small beam size as well as a minimum value of betatron functions in the device center. However, such systems require longer gaps in order to introduce additional lenses.

The contribution of the wiggler field to the dependence of the betatron oscillation frequencies on the betatron oscillation amplitudes can also be obtained from Hamiltonian (51). For this, we switch to action–phase variables $(x, y) \to (J_x, \phi_x, J_y, \phi_y)$ in the third brackets in the standard way:

$$u = \sqrt{2J_u\beta_u}\cos(\phi_u + \phi_0)\,, \quad u = x, y\,,$$

and find the frequency correction

$$\Delta\nu_u(J_x, J_y) = \left\langle \frac{\partial H}{\partial J_u} \right\rangle_{\phi_u}\,,$$

where angular brackets denote averaging over the corresponding phase variable, resulting in the expressions

$$\Delta\nu_x = \alpha_{xx}J_x + \alpha_{xy}J_y\,, \quad \Delta\nu_y = \alpha_{xy}J_x + \alpha_{yy}J_y\,,$$

$$\alpha_{xx} = \frac{L_\mathrm{w}}{8\pi}\,k_x^4\theta_\mathrm{m}^2\bar{\beta}_x^2\,, \quad \alpha_{xy} = \frac{L_\mathrm{w}}{4\pi}\,k_\mathrm{w}^2k_x^2\theta_\mathrm{m}^2\bar{\beta}_x\bar{\beta}_y\,,$$
$$\alpha_{yy} = \frac{L_\mathrm{w}}{8\pi}\,k_y^4\theta_\mathrm{m}^2\bar{\beta}_y^2\,. \tag{55}$$

Just as for the betatron-oscillation frequency shift (54), only the vertical frequency depends on the amplitude in the case of infinitely wide wiggler poles ($k_x = 0$). The expression for the cubic nonlinearity per undulator period in this case has the simple form

$$\alpha_{yy} = \frac{1}{2}\,k_\mathrm{w}\left(\frac{\bar{\beta}_y}{r}\right)^2.$$

6.2 Damping wigglers

Additional radiation from wigglers increases the radiation reaction force and can also lead to a reduction in beam emittance, depending on the parameters of the snake (as wigglers are sometimes called) and the optical functions in the region where the snake is located.

Using the formalism of structure (radiative) integrals introduced in [52], the emittance of a relativistic electron beam related to synchrotron radiation can be expressed as

$$\varepsilon_x = \frac{55\hbar}{32\sqrt{3}mc}\,\frac{\gamma^2}{J_x}\,\frac{I_5}{I_2} = \frac{55\hbar}{32\sqrt{3}mc}\,\frac{\gamma^2}{J_x}\,\frac{\oint \mathrm{d}s H(s)/|r|^3}{\oint \mathrm{d}s\,1/r^2}\,, \tag{56}$$

where $\hbar$ is the Planck constant, J_x the dimensionless damping rate of horizontal betatron oscillations (we assume $J_x = 1$ in what follows), r the curvature radius of the orbit, and function $H(s)$ is determined by the behavior of optical ($\alpha_x, \beta_x, \gamma_x$ are the Twiss parameters) and dispersion η_x functions in bending magnets,

$$H = \gamma_x\eta_x^2 + 2\alpha_x\eta_x\eta_x' + \beta_x\eta_x'^2\,, \tag{57}$$

where the prime denotes a derivative with respect to the longitudinal coordinate s. The integrals in (56) can be taken separately over the magnets of the ring and over the wigglers: $I_n = I_{n0} + I_{n\mathrm{w}}$. Then the relative contribution of wigglers to the total emittance becomes

$$r_\varepsilon = \frac{\varepsilon_x}{\varepsilon_{x0}} = \frac{1 + I_{5\mathrm{w}}/I_{50}}{1 + I_{2\mathrm{w}}/I_{20}}\,. \tag{58}$$

As is shown below, for an effective reduction of emittance, devices with a large field amplitude and small period are needed. In addition, we assume that the wiggler poles are wide enough in the transverse direction for the dependence of the field on the x coordinate to be neglected. For such devices, the vertical field along the axis can be expressed as $B_y = B_0\cosh(k_\mathrm{w}y)\cos(k_\mathrm{w}z)$. Now, neglecting the contributions of edge wiggler poles, we consider the periodic part only. The dispersion function and its derivative, driven by a periodic wiggler field, then have the form

$$\eta_\mathrm{w}(z) = \frac{1 - \cos(k_\mathrm{w}z)}{k_\mathrm{w}^2 r} = \eta_{\mathrm{w}0} - \frac{\theta_\mathrm{m}\cos(k_\mathrm{w}z)}{k_\mathrm{w}}\,,$$
$$\eta_\mathrm{w}'(z) = \frac{\sin(k_\mathrm{w}z)}{k_\mathrm{w}r} = \theta_\mathrm{m}\sin(k_\mathrm{w}z)\,. \tag{59}$$

The term $\eta_{\mathrm{w}0}$ in (59) can contain both the wiggler's own constant part of the dispersion function and the average value of residual dispersion in the straight section of the ring.

[8] The abbreviation FODO stands for a periodical system for focusing of charged particles that travel along some straight line, chosen to be the z axis. Every period of the system consists of a magnetic quadrupole lens F, empty gap O, magnetic quadrupole lens D, and second empty gap O. Usually, quadrupole lenses F and D are geometrically identical, but the magnetic field that they produce at corresponding points has opposite directions. Lens F focuses (returns to the z axis) particles with trajectories that lie in the horizontal plane xz and defocuses the ones with trajectories in the vertical plane yz. Lens D defocuses particles with trajectories that lie in the horizontal plane xz and focuses the ones with trajectories in the vertical plane yz.

In (57), we substitute the value of the function $\beta_x(z) = \bar{\beta}_x$ averaged over the wiggler length. For the sinusoidal wiggler model, we can then find the radiative integrals

$$I_{5w} \approx \frac{8}{15} N\theta_m h_w^2 \left(\frac{5\eta_{w0}^2}{\bar{\beta}_x} + \bar{\beta}_x \theta_m^2 \right), \quad I_{2w} = \frac{L h_w^2}{2}, \tag{60}$$

where $h_w = 1/r$ is the maximum curvature of the trajectory in the wiggler. The expression for I_{5w} shows only terms of the lowest order in the rotation angle $\theta_m \ll 1$ (other terms are neglected as small). The value of the fifth integral I_{5w} in (60) reaches its minimum at $\eta_{w0} = 0$. But because it is not possible to exactly set the dispersion function to zero in the straight section, it is reasonable to set the practical limit for which the influence of the residual dispersion on the resulting emittance is small:

$$\eta_{w0} \ll \frac{\bar{\beta}_x \theta_m}{\sqrt{5}}.$$

With this condition taken into account, the fifth radiation integral of the wiggler takes the form

$$I_{5w} \approx \frac{8}{15} N\theta_m^3 h_w^2 \bar{\beta}_x = \frac{1}{15\pi^3} \lambda_w^3 h_w^5 L \bar{\beta}_x.$$

Substituting I_{5w} and I_{2w} in (58), we obtain the well-known expression (see, e.g., [34])

$$r_\varepsilon = \frac{\varepsilon_x}{\varepsilon_{x0}} \approx \frac{1 + h_w^5 N \lambda_w^3 \bar{\beta}_x / (15\pi^3 I_{50})}{1 + h_w^2 N \lambda_w / (2 I_{20})}. \tag{61}$$

Figure 22 shows the typical behavior of the function r_ε in (58) depending on the wiggler field $B_0 \sim h_w$. For a fixed field period, the emittance $r_\varepsilon(B_0)$ has a typical minimum at some B_{opt}. The emittance increases together with the field amplitude. The value $h_{w\,opt}$ can be found using the assumption that the radiative damping is mostly determined by wigglers: $I_{2w} \gg I_{20}$. We can then neglect the constant in the denominator of (58):

$$h_{w\,opt} = \left(\frac{10\pi^3 I_{50}}{\lambda_w^2 L \bar{\beta}_x} \right)^{1/5} \approx \pi \left(\frac{I_{50}}{\lambda_w^2 L \bar{\beta}_x} \right)^{1/5}.$$

Moreover, the minimum emittance depends on only one parameter, period λ_w:

$$r_{\varepsilon\,min} \approx \frac{8}{3} \frac{I_{20}}{\pi^2 L^{3/5}} \left(\frac{\bar{\beta}_x \lambda_w^2}{I_{50}} \right)^{2/5}.$$

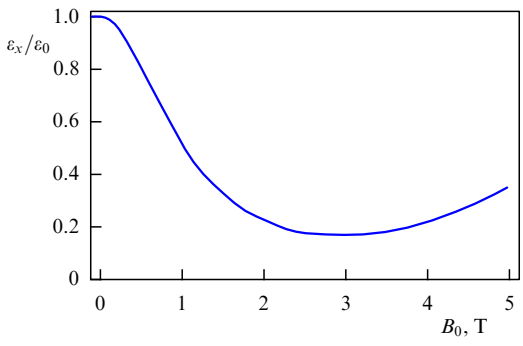

Figure 22. Relative variation of the beam emittance caused by the wiggler influence.

It follows from (61) that for an effective emittance reduction the wiggler must significantly increase the damping (the integral I_{2w}). For a fixed total length of wigglers defined by the dimensions of the setup, we can increase I_{2w} in (60) only by increasing the magnetic field amplitude h_w. On the other hand, in order to decrease the emittance, the condition $I_{5w} < I_{50}$ must be satisfied, which can be achieved, as we can see from the numerator in (61), by decreasing λ_w. These two requirements are contradictory, because the amplitude and the period are related as $B_0 \sim \exp(-\pi g/\lambda_w)$.

In the software for modeling particle motion in cyclic accelerators, the magnets are usually approximated by piecewise-constant functions. For reference, we write the second and fifth integrals in the case where the wiggler magnets are defined as a piecewise-constant function:

$$I_{2w}^{pw} = L h_w^2, \quad I_{5w}^{pw} \approx \frac{1}{48} \lambda_w^2 h_w^5 L \bar{\beta}_x.$$

The second radiation integral in the piecewise-constant approximation is two times larger than in the sinusoidal model for the wiggler field, but the fifth integral is $15\pi^3/48 \approx 10$ times larger as well, and this should be taken into account when calculating the wiggler influence on the radiation parameters of the beam.

6.3 Wiggler optimization and the gap optics

The value of the integral I_{5w} in (60) is mostly determined by the average value of the horizontal betatron function β_x in the wiggler gap. Therefore, the behavior of this function can be optimized in such a way that its average over the length value would be minimal. Then I_{5w} (60) reaches its maximum value.

Such a procedure is similar to optical function optimization in the bending magnets of an SR source in order to decrease the emittance. We present optimization results for two common cases of wiggler arrangement [53]:

- Wiggler cell has the above-mentioned simplest FODO structure.
- Behavior of optical functions is mirror-symmetric with respect to the wiggler center.

In FODO, a wiggler is installed between two lenses: focusing and defocusing. Such a cell is the most compact one, and therefore if the total length of the wiggler is several tens or hundreds of meters, the FODO structure can help to significantly decrease the size of the whole setup. Figure 23 shows a FODO cell that includes two wigglers.

For an estimation, we assume that quadrupole lenses are thin and have equal optical power moduli, while the space between them is occupied with the wiggler in such a way that the FODO cell length is $L_c \approx 2L$. The behavior of betatron functions in this structure is well known and we can obtain the following expression for the fifth integral:

$$I_{5w}^{FODO} \approx \frac{8}{15} N\theta_m^3 h_w^2 L F(\mu_x), \tag{62}$$

where the function $F(\mu_x)$ describes the dependence of the fifth integral on the shift of the horizontal betatron phase (Fig. 24):

$$F(\mu_x) = \frac{2}{3} \operatorname{cosec} \mu_x \left[2 + \cos^2 \left(\frac{\mu_x}{2} \right) \right]. \tag{63}$$

This function reaches its minimum when

$$\sin \left(\frac{\mu_{x\,opt}}{2} \right) = \sqrt{\frac{3}{5}}, \quad \mu_{x\,opt} \approx 101.5^\circ, \quad F_{opt} = \frac{4}{\sqrt{6}} \approx 1.63.$$

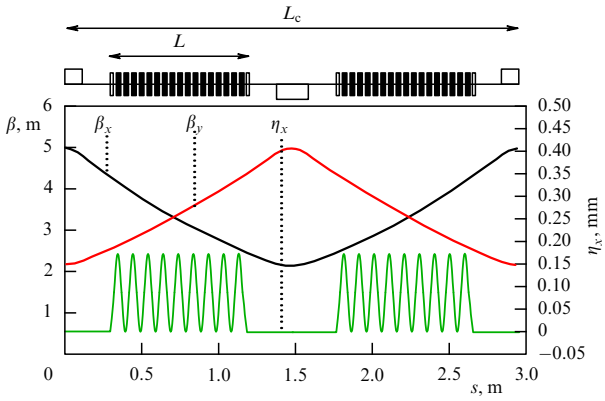

Figure 23. Two wigglers with a length L installed in the FODO optical cell with a length L_c. The plot shows betatron functions and the dispersion function η_x calculated using MAD8 software (http://mad8.web.cern.ch/mad8/).

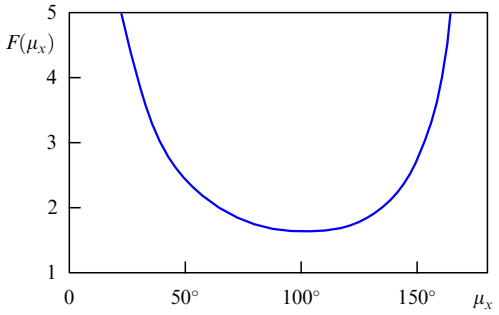

Figure 24. Function $F(\mu_x)$ in (63) versus the betatron phase shift over the FODO cell.

Using the known optimal shift of the betatron phase, it is easy to find the maximum value of the horizontal betatron function $\hat{\beta}_x$ in the focusing lens together with the value $\bar{\beta}_x$ averaged over the lens length:

$$\hat{\beta}_x = \frac{5}{\sqrt{6}}\left(1+\sqrt{\frac{3}{5}}\right)L \approx 3.62L\,, \quad \bar{\beta}_x = 2\sqrt{\frac{2}{3}}L \approx 1.63L\,. \tag{64}$$

Expressions (64) define the conditions for the wiggler length L to match the horizontal betatron function of the FODO cell. If these conditions are satisfied, the wiggler field contribution to the radiative excitation of emittance is suppressed in the most effective way. In this case, the fifth integral reaches its minimum:

$$I_{5w\,\min}^{\mathrm{FODO}} = \frac{16\sqrt{2}}{15\sqrt{3}}\,Nh_w^2\theta_m^3 L\,. \tag{65}$$

It is interesting to note that the dependence of the fifth integral in (65) produced by the wiggler is similar to the dependence of the fifth integral produced by the bending magnet in the FODO cell. However, in the latter case, the dependence reaches its minimum when $\mu_{x\,\mathrm{opt}} \approx 137^\circ$ (the problem of natural emittance minimization in the FODO structure was discussed, e.g., in [54]).

It is known that the FODO structure is not optimal for emittance minimization in SR sources. A minimal emittance can be obtained in the TME-type structure (theoretical minimum emittance), where optical functions are mirror-symmetric with respect to the magnet center and $\beta_x(s)$ and $\eta_x(s)$ reach minimums in this point (Fig. 25).

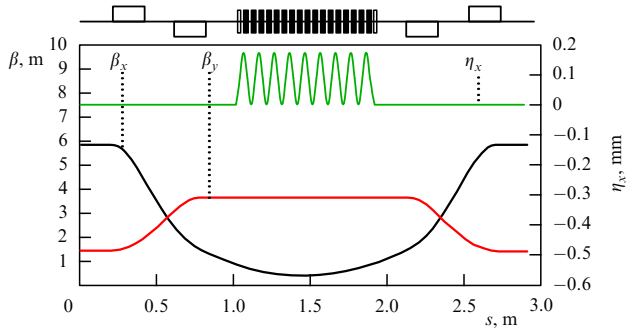

Figure 25. Wiggler installed in a TME-type cell (upper part of the figure). Betatron functions and the dispersion function η_x calculated using MAD8 software.

We assume that $\beta_x(L/2) = \beta_{x0}$ and $\alpha_x(L/2) = 0$ at the central point of the snake. Neglecting wiggler focusing, after the corresponding integration, we can obtain the fifth integral in the form

$$I_{5w}^{\mathrm{TME}} \approx \frac{8}{15}\,N\theta_m^3 h_w^2\left(\beta_{x0} + \frac{L^2}{12\beta_{x0}}\right).$$

By minimizing the last expression, we obtain

$$I_{5w\,\min}^{\mathrm{TME}} \approx \frac{8}{15}\,N\theta_m^3 h_w^2\,\frac{L}{\sqrt{3}} \quad \text{for} \quad \beta_{x0\,\mathrm{opt}} = \frac{L}{2\sqrt{3}}\,. \tag{66}$$

If we compare this expression with the corresponding expression (65) for the FODO structure,

$$I_{5w\,\min} \approx N\theta_m^3 h_w^2 L \begin{cases} \dfrac{8}{15}\,\dfrac{2\sqrt{2}}{\sqrt{3}}\,, & \mathrm{FODO}\,, \\ \dfrac{8}{15}\,\dfrac{1}{\sqrt{3}}\,, & \mathrm{TME}\,, \end{cases}$$

we can see that in the TME structure with the same wiggler length, we can achieve a value that is $2\sqrt{2}$ times the fifth integral. However, it should be remembered that the number of quadrupole lenses is smaller in the FODO case than in the TME case. This means that in the FODO case the distances between snakes are larger and therefore their 'linear density' is smaller.

6.4 Wiggler period modulation

The fifth radiation integral over the wiggler length can be expressed in the form

$$I_{5w} = \int_0^L H(z)\,|h(z)|^3\,\mathrm{d}z\,.$$

It can be shown that the maximum contribution to the function $H(z)$ is made by the term $H(z) \approx \beta_x(z)\,\eta_z'^2(z)$. Considering the TME case for simplicity, we obtain

$$I_{5w} \approx 2\int_0^{L/2}\left(\beta_{x0} + \frac{z^2}{\beta_{x0}}\right)\left|\cos\left(\frac{2\pi}{\lambda_w}\,z\right)\right|^5 h_w^5\,\frac{\lambda_w^4}{(2\pi)^4}\,\mathrm{d}z\,. \tag{67}$$

The function in the integrand in (67) can be separated into two parts: one that is periodic in z and is related to the snake

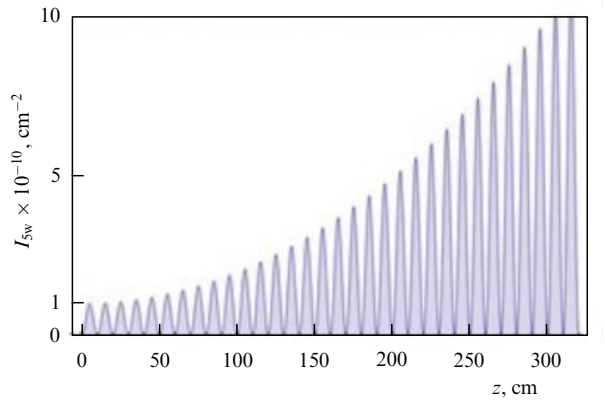

Figure 26. Integrand from (67). The origin corresponds to the snake center.

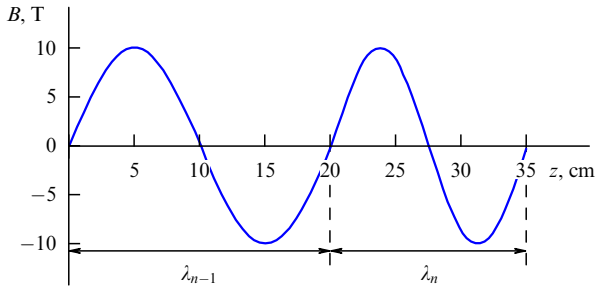

Figure 27. Decrease in the wiggler period.

field and one that increases as $\sim z^2$, being connected with the betatron function. The characteristic form of the integrand in (67) is shown in Fig. 26.

We can compensate the increase in $\beta_x(z)$ together with z by reducing the wiggler period length $\lambda_w = \lambda_w(z)$, as shown in Fig. 27.

The considered method goes back to A Wrulich's idea, which he introduced in 1992 (see, e.g., [55–57]). According to this idea, an increase in the $H(s)$ function in a bending magnet can be compensated by decreasing the magnetic field. Such magnets were later named 'longitudinal gradient magnets'. In our case, it is undesirable to decrease the field amplitude, because this would reduce the second integral I_{2w} in the denominator of emittance expression (56). Then, despite reducing I_{5w}, the emittance can increase. But because I_{2w} does not depend on the wiggler period, the period can be decreased at least down to values that do not significantly influence the field amplitude in the gap of the periodic magnet.

Using the reasonable assumption $\lambda_w \ll \bar{\beta}_x$, a recurrent expression was obtained in [53] for the nth wiggler period in terms of the length of the $(n-1)$th period,

$$\lambda_n \approx \lambda_{n-1}\left(1 + \frac{2\,\alpha_{x,n-1} d_{n-1}}{3 - 10\,\alpha_{x,n-1} d_{n-1}}\right), \tag{68}$$

where $d_{n-1} = \lambda_{n-1}/\beta_{x,n-1}(0)$, $\alpha_{x,n-1}(0)$, and $\beta_{x,n-1}(0)$ are the initial values of the Twiss parameters at the beginning of the considered period, which can be easily calculated for the straight section (weak focusing of the wiggler is neglected here).

The variation of the period in the example shown in Fig. 26 leads to a significant decrease in $\mathrm{d}I_{5w}/\mathrm{d}z$ (Fig. 28), and the value of the radiation integral decreases fourfold.

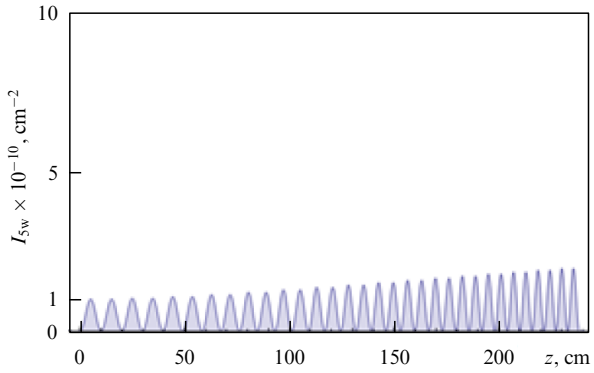

Figure 28. Integrand in (67) with the snake period variation taken into account in accordance with (68).

An insignificant increase in the integrand in Fig. 28 at the snake end is explained by the fact that expression (68) is still an approximate one.

7. Conclusions

In this review, we tried to answer those questions associated with wigglers and undulators which were not addressed in previous reviews on this topic. As that any experimental work that includes physical, technological, theoretical, and application aspects, the presented material is quite diverse. Therefore, we hope that readers with various scientific interests will find something interesting for them in our review.

Acknowledgments
This work was supported by the Russian Scientific Fund (project 14-50-00080). The authors are grateful to E A Perevedentsev for showing us the pioneering work by V P Ermakov (references are given in the Appendix)

8. Appendix. Motion of electrons in circular accelerators

In this review, we use results of the cyclic accelerator theory (see, e.g., books [32–34]). We briefly discuss some of these results.

We consider a magnetic system of a cyclic accelerator with a scalar magnetic potential that is antisymmetric with respect to some plane, called the median plane. Under some conditions that we do not discuss in detail, closed trajectories (orbits) exist in the median plane for particles with a specific energy. It is convenient to define a particle that moves along a closed orbit as a 'reference' one and describe the motion of particles with other initial conditions in terms of coordinate and momentum deviations from the corresponding values of the reference particle. A necessary condition for a cyclic accelerator to work is the existence of a stable closed orbit. If an orbit is stable, particles with small deviations from the reference stay in the vicinity of this orbit for an 'infinitely long time'. Small deviations of their trajectories from the median plane y (vertical deviation) and along the principal normal to the orbit $-x$ (horizontal deviation) are described by the linearized trajectory equations

$$\begin{aligned} x'' + K_x(s)\,x &= 0\,, \\ y'' + K_y(s)\,y &= 0\,, \end{aligned} \tag{A1}$$

where the stiffnesses are expressed as $K_x = 1/r^2 + (e/pc)\,\partial B_y/\partial x$, $K_y = -(e/pc)\,\partial B_y/\partial x$, $1/r = eB_y/pc$, s is the length along the orbit (we use the natural parameterization), and differentiating with respect to s is denoted by a prime. The term $1/r^2$ arises in the expression for stiffness because our reference frame is curvilinear (locally, it is cylindrical with coordinates $R = r + x$, $\alpha = s/r$, and $z = y$), and the generalized coordinate axes rotate as s is varied. If the length (circumference) of the orbit is Π, then both stiffnesses are periodic functions with this period. Linear differential equations (A1) with periodic coefficients are known as Hill equations. Their solution can be written in the form [58, 59]

$$x = Aw_x(s)\,\cos\left(\int_0^s \frac{\mathrm{d}s_1}{w_x^2} + \varphi_0\right), \tag{A2}$$

where A and φ_0 are arbitrary constants that depend on the initial conditions, and w_x is a periodic function that satisfies the equation

$$w_x'' + K_x(s)\,w_x - \frac{1}{w_x^3} = 0\,. \tag{A3}$$

The function w_x, which does not depend on initial conditions, characterizes the focusing system (bending magnets and quadrupole lenses) of a given cyclic accelerator. Therefore, solutions of Hill equation (A2) depend on the initial conditions in a simple way, expressed by the initial amplitude A and phase φ_0.

We assume that we measure the coordinate x and the angle x' of the particle when it passes through the plane that is perpendicular to the orbit and crosses it at some coordinate s. After every turn of the particle in the accelerator, the phase in (A2) increases by

$$\mu_x = 2\pi\nu_x = \int_0^{\Pi} \frac{\mathrm{d}s}{w_x^2}\,, \tag{A4}$$

which is called the betatron phase advance. The parameter ν_x is called the betatron frequency. It follows from (A2) that points on the phase plane with the coordinate $x_n = Aw_x\cos(n\mu_x + \varphi_1)$ and the angle (or the dimensionless transverse momentum) $x_n' = Aw_x'\cos(n\mu_x + \varphi_1) - A\sin(n\mu_x + \varphi_1)/w_x$ on the phase plane xx', fill an ellipse during the particle revolution:

$$\beta_x x'^2 + 2\alpha_x x x' + \gamma_x x^2 = A^2\,. \tag{A5}$$

The parameters

$$\beta_x = \frac{2\langle x^2\rangle}{A^2} = \frac{x_{\max}^2}{A^2} = w_x^2\,, \quad \alpha_x = -\frac{2\langle xx'\rangle}{A^2} = -w_x w_x'\,,$$
$$\gamma_x = \frac{2\langle x'^2\rangle}{A^2} = \frac{x'_{\max}}{A^2} = w_x'^2 + \frac{1}{w_x^2}$$

are called the Twiss parameters (angular brackets denote averaging over time or, in other words, over n). Because the oscillation amplitude $x_{\max}(s) = Aw_x(s)$ is also the envelope of the full trajectory (A2), w_x is called the normalized envelope.

To compensate the radiative energy losses, electron circular accelerators have a gap with an alternating longitudinal electric field that varies in time harmonically. The reference particle can be chosen as the one that passes through the accelerating gap exactly at the instant when the energy increment due to the gap field coincides with the energy losses per cycle. The reference particle trajectory is closed only when the reference particle energy is always the same after passing the accelerating gap. This requires that the reference particle revolution period Π/v is a multiple of the accelerating field period. Because the particle revolution period depends on its energy, the energy of the reference particle is determined from the condition for the revolution period to be a multiple of the gap field period. If the initial energy or arrival time of the electron slightly differ from the corresponding parameters of the reference particle, the delay in the gap passing time and the energy deviation oscillate. The oscillations are called synchrotron oscillations and the fact that these oscillations are stable is called the autophasing principle. The delay, then plays the role of a coordinate and the energy deviation plays the role of momentum. The deflection $x = \eta(s)\,\Delta p/p$ of a closed orbit with the energy deviation $\Delta E/E \approx \Delta p/p$ from a reference closed orbit is described by a periodic function η that is a solution of the equation

$$\eta'' + K_x(s)\,\eta = \frac{1}{r(s)}\,. \tag{A6}$$

Betatron and synchrotron oscillations are damped due to the radiation reaction force. It is easier to describe the damping of vertical betatron oscillations. Because the radiation reaction force is directed along the velocity, its vertical projection $F_y = y'P/v = y'2e^2\beta^3\gamma^4/(3r^2)$ can be expressed in terms of the radiation power P. This gives rise to the 'friction' term in the second equation in (A1) for the vertical deviation of the trajectory:

$$y'' + \frac{2r_e\gamma^3}{3r^2}\,y' + K_y y = 0\,, \tag{A7}$$

where $r_e = e^2/(mc^2)$ is the classical electron radius. Because this friction force is small, Eqn (A7) can be solved using the method of variation of parameters, applied to solution (A2). As a result, we find that during one revolution period, the amplitude of betatron oscillations decreases by the factor $\exp(r_e\gamma^3 I_2/3)$, where $I_2 = \int_0^{\Pi} \mathrm{d}s/r^2(s)$. The damping of horizontal betatron oscillations and synchrotron oscillations is calculated similarly. However, due to the transverse dependence of the magnetic field $\partial B_y/\partial x$, the radiation power can depend on the full horizontal deviation of the trajectory,

$$x = Aw_x(s)\,\cos\left(\int_0^s \frac{\mathrm{d}s_1}{w_x^2} + \varphi_0\right) + \eta(s)\,\frac{\Delta E}{E}\,. \tag{A8}$$

Therefore, these two degrees of freedom are coupled, and the damping rates can be redistributed between them. Such a redistribution is used in the Robinson wiggler, mentioned in the Introduction.

The radiative energy losses occur instantaneously by emitting single quanta with energy $\hbar\omega$, which increases the oscillations. Because the photon energy is small, this effect leads to velocity diffusion. In the case of horizontal transverse motion, the oscillations are increased in the following way. The electron with an energy E initially moves exactly along a closed orbit (that is, with zero betatron oscillation amplitude), but after instantaneously losing the energy $\hbar\omega$, the electron immediately acquires the coordinate deviation $x = \eta(s)\,\hbar\omega/E$ with the angular deviation $x' = \eta'(s)\,\hbar\omega/E$ from its new

closed orbit with the energy $E-\hbar\omega$. After this, the electron starts to perform betatron oscillations around its new orbit. According to (A5), the squared amplitude of these oscillations is

$$A^2=(\beta_x\eta'^2+2\alpha_x\eta\eta'+\gamma_x\eta^2)\left(\frac{\hbar\omega}{E}\right)^2.$$

The horizontal diffusion coefficient averaged over the revolution period (that is, the increase rate of the average squared oscillation amplitude) is proportional to

$$I_5=\int_0^{\Pi}\frac{\beta_x\eta'^2+2\alpha_x\eta\eta'+\gamma_x\eta^2}{r^3}\,\mathrm{d}s\,. \tag{A9}$$

The average photon energy of synchrotron radiation is proportional to the field, which gives $1/r$, and the radiation power is proportional to $1/r^2$. Therefore, the denominator in (A9) is r^3. The effects of excitation (due to quantum fluctuations of radiation) and damping result in a Gaussian distribution of electrons over all three degrees of freedom.

The dimensions of an electron bunch that circulates in the circular accelerator depend on the longitudinal coordinate s on the orbit. Therefore, it is convenient to characterize the bunch using invariant combinations (independent of s) of the particle distribution second moments. For example, the value

$$\varepsilon_y=\sqrt{\langle y^2\rangle\langle y'^2\rangle-\langle yy'\rangle^2}\,, \tag{A10}$$

where the angular brackets denote averaging over all particles of the bunch, is called the vertical emittance (roughly speaking, it is just the product of the size and the angular spread). Then the root mean square size of the bunch in the plane that is perpendicular to the orbit and crosses it at the point with the coordinate s is given by $\sqrt{\langle y^2\rangle}=\sqrt{\varepsilon_y}w_y(s)$. Because the closed orbit of particles with the energy deviation ΔE is shifted with respect to the reference orbit, the horizontal emittance involves the particle deviation from the orbit:

$$\varepsilon_x=\left[\left\langle\left(x-\eta(s)\,\frac{\Delta E}{E}\right)^2\right\rangle\left\langle\left(x'-\eta'(s)\,\frac{\Delta E}{E}\right)^2\right\rangle-\left\langle\left(x-\eta(s)\,\frac{\Delta E}{E}\right)\left(x'-\eta'(s)\,\frac{\Delta E}{E}\right)\right\rangle^2\right]^{1/2}. \tag{A11}$$

The transverse size and angular spread decrease as the transverse emittances are reduced. The friction force allows minimizing transverse emittances, and this is required in many cases. For example, in electron–positron colliders, luminosity can be increased, and in X-ray radiation sources, brightness can be increased. Positrons are produced by scattering electrons with energies of the order of 100 MeV on a heavy-metal target. In this case, the energy spread, the angular divergence, and the transverse size of the positron beam (and both emittances as well) are quite large. These parameters can be decreased by injecting positrons into the cyclic accelerator (or the so-called storage ring, which has a constant field), waiting until the emittances decrease, and directing the 'cooled' positrons to the electro-optical channel for further use (for example, in linear or cyclic colliders). Specialized storage rings that are used to reduce the emittances and energy spread of the particles are called damping rings.

References

1. Ginzburg V L *Izv. Akad. Nauk SSSR Ser. Fiz.* **11** (2) 165 (1947)
2. Motz H *J. Appl. Phys.* **22** 527 (1951)
3. Motz H, Thon W, Whitehurst R N *J. Appl. Phys.* **24** 826 (1953)
4. Robinson K W *Phys. Rev.* **111** 373 (1958)
5. Tischer M et al., in *Proc. of the 2005 IEEE Particle Accelerator Conf., PAC'05, 16–20 May 2005, Knoxville, Tennessee. 21st IEEE Particle Accelerator Conf.* (Piscataway, NJ: IEEE, 2005) p. 2446
6. Landau L D, Lifshitz E M *The Classical Theory of Fields* (Oxford: Pergamon Press, 1980); Translated from Russian: *Teoriya Polya* (Moscow: Nauka, 1973)
7. Feynman R, Leighton R, Sands M *The Feynman Lectures on Physics* Vol. 2 (Reading, Mass.: Addison-Wesley Publ. Co., 1964); Translated into Russian: *Feinmanovskie Lektsii po Fizike* Vol. 2 (Moscow: Mir, 1965)
8. Litvinenko V N et al. *Phys. Rev. Lett.* **78** 4569 (1997)
9. Nedorezov V G, Turinge A A, Shatunov Yu M *Phys. Usp.* **47** 341 (2004); *Usp. Fiz. Nauk* **174** 353 (2004)
10. Bychenkov V Yu et al. *Phys. Usp.* **58** 71 (2015); *Usp. Fiz. Nauk* **185** 77 (2015)
11. Kostyukov I Yu, Pukhov A M *Phys. Usp.* **58** 81 (2015); *Usp. Fiz. Nauk* **185** 89 (2015)
12. Kulipanov G N, Skrinskii A N *Sov. Phys. Usp.* **20** 559 (1977); *Usp. Fiz. Nauk* **122** 369 (1977)
13. Ternov I M *Phys. Usp.* **38** 409 (1995); *Usp. Fiz. Nauk* **165** 429 (1995)
14. Kulipanov G N *Phys. Usp.* **50** 368 (2007); *Usp. Fiz. Nauk* **177** 384 (2007)
15. Bessonov E G, Vinogradov A V *Sov. Phys. Usp.* **32** 806 (1989); *Usp. Fiz. Nauk* **159** 143 (1989)
16. Alferov D F, Bashmakov Yu A, Cherenkov P A *Sov. Phys. Usp.* **32** 200 (1989); *Usp. Fiz. Nauk* **157** 389 (1989)
17. Jackson J D *Classical Electrodynamics* 3rd ed. (New York: Wiley, 1999)
18. Clarke J A *The Science and Technology of Undulators and Wigglers* (Oxford: Oxford Univ. Press, 2004)
19. Vinokurov N *Rev. Accel. Sci. Technol.* **3** 77 (2010)
20. Levichev E, Vinokurov N *Rev. Accel. Sci. Technol.* **3** 203 (2010)
21. Hoyer E et al. (representing the Beam Line VI Design Group) *Nucl. Instrum. Meth. Phys. Res.* **208** 117 (1983)
22. Kornyukhin G A et al. *Nucl. Instrum. Meth. Phys. Res.* **208** 189 (1983)
23. Kornyukhin G A et al. *Nucl. Instrum. Meth. Phys. Res. A* **237** 281 (1985)
24. Chavanne J, Van Vaerenbergh P, Elleaume P *Nucl. Instrum. Meth. Phys. Res. A* **421** 352 (1999)
25. Fedurin M G et al. *Nucl. Instrum. Meth. Phys. Res. A* **470** 34 (2001)
26. Halbach K *Nucl. Instrum. Meth. Phys. Res.* **187** 109 (1981)
27. Elias L R et al. *Opt. Commun.* **18** 129 (1976)
28. Elias L R, Madey J M *Rev. Sci. Instrum.* **50** 1335 (1979)
29. Artamonov A S et al. *Nucl. Instrum. Meth. Phys. Res.* **177** 239 (1980)
30. Ingold G et al. *Nucl. Instrum. Meth. Phys. Res. A* **375** 451 (1996)
31. Rossmanith R et al., in *Proc. of the 2003 IEEE Particle Accelerator Conf., PAC'03, 12–16 May 2003, Portland, Oregon, 20th IEEE Particle Accelerator Conf.* (Piscataway, NJ: IEEE, 2003) p. 899
32. Kolomensky A A, Lebedev A N *Theory of Cyclic Accelerators* (Amsterdam: North-Holland, 1966); Translated from Russian: *Teoriya Tsiklicheskikh Uskoritelei* (Moscow: Fizmatgiz, 1962)
33. Lebedev A N, Shal'nov A V *Osnovy Fiziki i Tekhniki Uskoritelei* (Basics of Accelerator Physics and Technology) (Moscow: Energoatomizdat, 1991)
34. Chao A W, Tigner M *Handbook of Accelerator Physics and Engineering* (Singapore: World Scientific, 1999)
35. Sands M *Phys. Rev.* **97** 470 (1955)
36. Kolomenskii A A, Lebedev A N *Sov. Phys. JETP* **3** 132 (1956); *Zh. Eksp. Teor. Fiz.* **30** 207 (1956)
37. Pinayev I V et al. *Nucl. Instrum. Meth. Phys. Res. A* **341** 17 (1994)
38. Aleshaev A N et al. *Nucl. Instrum. Meth. Phys. Res. A* **359** 80 (1995)
39. Pinayev I V et al. *Nucl. Instrum. Meth. Phys. Res. A* **375** 71 (1996)
40. Shaftan T V, PhD Thesis Phys.-Math. Sci. (Novosibirsk: Budker INP SB RAS, 1997)
41. Faleev S V *JETP* **84** 856 (1997); *Zh. Eksp. Teor. Fiz.* **111** 1563 (1997)
42. Faleev S V, hep-ph/9706372

43. Bekhtenev E A et al. *Phys. Part. Nucl. Lett.* **3** S16 (2006); *Pis'ma Fiz. Elem. Chast. At. Yad.* **3** 33 (2006)
44. Mezentsev N, in *Proc. of the 24th Russian Particle Accelerator Conf., RuPAC'2014, October 6 – 10, 2014, Obninsk, Russia* (Moscow: State Scientific Center of the Russian Federation, 2014) p. 296
45. Mezentsev N A, private communication (2014)
46. Landau L D, Lifshitz E M *Mechanics* (Oxford: Pergamon Press, 1976); *Mekhanika* (Moscow: Nauka, 1988)
47. Smith L, LBL Report LBL-21391 (Berkeley, CA: Lawrence Berkeley Laboratory, Univ. of California, 1986)
48. Gluskin E S et al. *Nucl. Instrum. Meth. Phys. Res. A* **475** 323 (2001)
49. Nikitina Yu M, Pflüger J *Nucl. Instrum. Meth. Phys. Res. A* **375** 325 (1996)
50. Rakowski J et al., in *Proc. of the 1999 Particle Accelerator Conf., March 27 – April 2, 1999, New York, USA* (Piscataway, NJ: IEEE, 1999) p. 2698
51. Brinkmann R et al. (Eds) "Conceptual Design of a 500 GeV e + e-Linear Collider with Integrated X-ray Laser Facility", DESY 1997-048, ECFA 1997-182, Vol. 2 (Hamburg: DESY, 1997)
52. Helm R H et al. *IEEE Trans. Nucl. Sci.* **20** 900 (1973)
53. Bogomyakov A, Karyukina K, Levichev E, in *Proc. of the 5th Intern. Particle Accelerator Conf., IPAC'14, Dresden, Germany, June 15 – 20, 2014*, p. 2038 – 2040
54. Helm R, Wiedemann H, Technical Report PEP-Note 303 (Menlo Park, CA: Stanford Linear Accelerator Center, 1979)
55. Wrulich A , private communication (1992)
56. Guo J, Raubenheimer T, in *Proc. of the 8th European Particle Accelerator Conf., June 3 – 7 2002, Paris, France* (Geneva: European Physical Society Interdivisional Group on Accelerators, CERN, 2002) p. 1136
57. Nagaoka R, Wrulich A F *Nucl. Instrum. Meth. Phys. Res. A* **575** 292 (2007)
58. Ermakov V P *Appl. Anal. Discrete Math.* **2** (2) 123 (2008); Translated from Russian: *Univ. Izv. Univ. sv. Vladimira, Kiev, otd. III* (9) 1 (1880)
59. Ermakov V P *Integrirovanie Differentsial'nykh Uravnenii* (Differential Equations Integrating) (Kiev: Litografiya L. G. Danilovoi, 1886)